SCIENCE CHINA
Technological Sciences

March 2012 Vol.55 No.3: 779–794
doi: 10.1007/s11431-011-4690-8

"Volume-point" heat conduction constructal optimization based on entransy dissipation rate minimization with three-dimensional cylindrical element and rectangular and triangular elements on microscale and nanoscale

FENG HuiJun, CHEN LinGen* & SUN FengRui

College of Naval Architecture and Power, Naval University of Engineering, Wuhan 430033, China

Received May 20, 2011; accepted November 10, 2011; published online January 20, 2012

Based on constructal theory, the constructs of three "volume-point" heat conduction models with three-dimensional cylindrical element and rectangular and triangular elements on microscale and nanoscale are optimized by taking minimum entransy dissipation rate as optimization objective. The optimal constructs of the three "volume-point" heat conduction models with minimum dimensionless equivalent thermal resistance are obtained. The results show that the optimal constructs of the three- dimensional cylindrical assembly based on the minimizations of dimensionless equivalent thermal resistance and dimensionless maximum thermal resistance are different, which is obviously different from the comparison between those of the corresponding two-dimensional rectangular assembly based on the minimizations of these two objectives. The optimal constructs based on rectangular and triangular elements on microscale and nanoscale when the size effect takes effect are obviously different from those when the size effect does not take effect. Because the thermal current density in the high conductivity channel of the rectangular and triangular second order assemblies are not linear with the length, the optimal constructs of these assemblies based on the minimization of entransy dissipation rate are different from those based on the minimization of maximum temperature difference. The dimensionless equivalent thermal resistance defined based on entransy dissipation rate reflects the average heat transfer performance of the construct. The studies on "volume-point" heat conduction constructal problems at three-dimensional conditions and microscale and nanoscale by taking minimum entransy dissipation rate as optimization objective extend the application range of the entransy dissipation extremum principle.

constructal theory, entransy dissipation rate, three-dimensional cylindrical element, microscale and nanoscale, volume-point heat conduction, generalized thermodynamic optimization

Citation: Feng H J, Chen L G, Sun F R. "Volume-point" heat conduction constructal optimization based on entransy dissipation rate minimization with three-dimensional cylindrical element and rectangular and triangular elements on microscale and nanoscale. Sci China Tech Sci, 2012, 55: 779–794, doi: 10.1007/s11431-011-4690-8

1 Introduction

"Volume-point" heat conduction problem is a class of common problem in constructal theory [1–6]. Many scholars have carried out constructal optimization on this problem through simplifying the three-dimensional "volume-point" heat conduction problem into the two-dimensional heat conduction problem [7–18]. Bejan obtained the optimal constructs of a "volume-point" heat conduction model based on rectangular element through assembling and by taking maximum temperature difference minimization as optimization objective [7]. Thenceforth, some scholars further reduced the heat residences of the constructs by opti-

*Corresponding author (email: lgchenna@yahoo.com; lingenchen@hotmail.com)

© Science China Press and Springer-Verlag Berlin Heidelberg 2012

mizing the width of the high conductivity channel of the rectangular element [8], getting rid of the perpendicular condition of the high and low conductivity channel [8], and adopting nonuniform arrangements of high conductivity materials [9]. Ghodoossi and Egrican [10] compared the exact and approximate solutions in ref. [7] by assumption that the thermal current in the high conductivity channel increased discontinuously, and found that the deviation between the two solutions was led by the simplification that the thermal current in the high conductivity channel increased continuously. Wu et al. [11] deeply analyzed the deviation, proved that this was not caused by the simplification of the thermal current distribution but by the inequivalent of the thermal conductivity coefficients based on energy conservation argument, and found that the conclusion derived by effective thermal conductivity based on the equivalent of maximum temperature difference agreed with the exact solution. On the basis of these work, some scholars tried to reduce maximum thermal resistances of the constructs by releasing the assumption that the new-order assembly should be assembled by the optimized last-order assembly [12], improving the shape of the elemental volume [13], and optimizing discrete variable cross-section high conductivity channel [14], variable cross-section high conductivity channels [15–17] as well as variable elemental shapes [16, 17]. Moreover, Karakas [18] adopted a different method to calculate the width of elemental volume, re-carried out constructal optimization of the model in ref. [7] by using Lagrange multiplier method, and obtained the new optimization results of the "volume-point" heat conduction problem.

In the "volume-point" heat conduction models above, simplification is made at the thermal current direction perpendicular to the surface of the control volume. However, these "volume-point" heat conduction models are immature due to this simplification. On consideration that the "volume-point" heat conduction problems actually should be three-dimensional ones, Ledezma and Bejan [19] built a three-dimensional "volume-point" heat conduction model with cylindrical high conductivity channel and cylindrical element, and obtained the optimal constructs of the three-dimensional cylindrical model by taking the minimization of maximum temperature difference as optimization objective. Neagu and Bejan [20] built a three-dimensional and finger-shaped "volume-point" heat conduction model with variable cross-section high conductivity channel and variable element, and obtained the optimal constructs of the high conductivity channel and variable element based on maximum temperature difference minimization. Alebrahim and Bejan [21] considered a three-dimensional "volume-point" heat conduction model with circular high conductivity channel and cylindrical element, and obtained the optimal constructs of the three-dimensional cylindrical model based on finite element method and by taking maximum temperature difference minimization as optimization objective.

The heat conduction problems above are carried out on conventional scale. However, when the size reduces to microscale and nanoscale, some new phenomena and laws will present in the microscale heat transfer processes [22–24], and some scholars have made plentiful work in this field [25–30]. In the analyses of the "volume-point" heat conduction constructal optimization problems, considering that the size effect will present in high conductivity material on microscale and nanoscale, Gosselin and Bejan [31] re-optimized Bejan's "volume-point" heat conduction model [7] by taking the minimization of maximum temperature difference as objective on microscale and nanoscale. The new optimal construct of the "volume-point" heat conduction model on unconventional scale was obtained, and the performance comparisons of the two optimal constructs on nanoscale and conventional scale were carried out.

However, the minimization of maximum temperature difference only reflects the heat transfer performance of a local one, not the global one of the models. Guo et al. [32, 33] put forward a new physical quantity, "entransy" (ever interpreted as heat transfer potential capacity in ref. [34]) and the extremum principle of entransy dissipation, and defined an equivalent thermal resistance for multi-dimensional heat conduction problems based on the entransy dissipation rate. The physical meaning of entransy was further expounded from the angles of heat conduction physical mechanism and electro-thermal simulation experiment, etc. [35–37]. On the basis of these work, some scholars further carried out a series of heat transfer optimizations by taking entransy dissipation rate minimization as optimization objective [38–52]. Wei et al. [53] firstly applied the extremum principle of entransy dissipation to the "volume- point" heat conduction constructal optimization problem, and found that the minimization of entransy dissipation rate was superior in reducing the average thermal resistance of the control volume to the minimization of maximum temperature difference. Furthermore, some scholars carried out constructal optimization of "volume-point" heat conduction models based on rectangular [54, 55], triangular [56] and variable shape [17] elements with different constraints as well as heat transfer models of electromagnet [57], geometries of cavity [58, 59], disc [60, 61], fins [62, 63], cooling channels [64], round tube heat exchanger [65] and steam generator [66]. The advantages of minimization of entransy dissipation rate for heat transfer optimizations are further illustrated.

On the basis of refs. [13, 21, 31], the "volume-point" heat conduction models with circular high conductivity channel and cylindrical element on convectional scale as well as rectangular and triangular elements on microscale and nanoscale will be re-optimized by taking entransy dissipation rate minimization as optimization objective, and the optimal constructs of the "volume-point" heat conduction models will be obtained. The work done in this paper will extend the application range of the entransy dissipation ex-

tremum principle.

2 Definition of entransy dissipation rate [32]

Entransy, which is a new physical quantity reflecting heat transfer ability of an object, was defined in ref. [32] as

$$E_{vh}=\frac{1}{2}Q_{vh}U_h=\frac{1}{2}Q_{vh}T, \quad (1)$$

where $Q_{vh}=Mc_vT$ is thermal capacity of an object with constant volume, U_h or T represents the thermal potential. The entransy dissipation function, which represents the entransy dissipation per unit time and per unit volume, is deduced as [32]

$$\dot{E}_{h\phi}=-\dot{q}\cdot\nabla T=k(\nabla T)^2, \quad (2)$$

where $\dot{q}$ is thermal current density vector, and ∇T is the temperature gradient. In steady-state heat conduction, $\dot{E}_{h\phi}$ can be calculated as the difference between the entransy input and the entransy output of the object, i.e.,

$$\dot{E}_{h\phi}=E_{h,\mathrm{in}}-E_{h,\mathrm{out}}. \quad (3)$$

The entransy dissipation rate of the whole volume in the "volume-to-point" conduction is

$$\dot{E}_{vh\phi}=\int_v \dot{E}_{h\phi}\mathrm{d}v=\int_v k(\nabla T)^2\mathrm{d}v. \quad (4)$$

The equivalent thermal resistance for multi-dimensional heat conduction problems with specified heat flux boundary condition is given as follows [32]:

$$R_h=\dot{E}_{vh\phi}\big/\dot{Q}_h^2, \quad (5)$$

where $\dot{Q}_h$ is the thermal current.

3 "Volume-point" heat conduction models

3.1 "Volume-point" heat conduction model with three-dimensional cylindrical element

A cylindrical element generates heat volumetrically (heat generation rate per unit volume is q''', and it is considered as a uniform internal heat source in the cylindrical element) as shown in Figure 1 [21]. The elemental volume V_0 (diameter H_1, length H_0, and $V_0=\pi H_1^2H_0/4$) is fixed, but the ratio H_0/H_1 is free to vary. The heat generated in the cylindrical element of k_0 material (isotropy) is collected by a disk-shaped insert of high thermal conductivity (k_p, D_0, H_1), and then flow to the heat sink located at point M_0 along the cylindrical high conductivity channel (k_p, D_1, H_0). The disk-shaped k_p material lies in middle section of the cylindrical

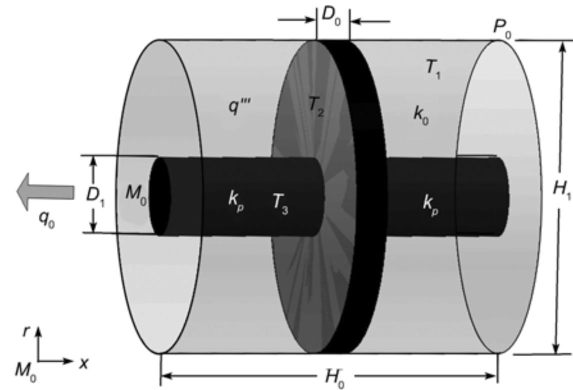

Figure 1 Cylindrical element [21].

high conductivity channel. The boundary of the cylindrical element is adiabatic except for the heat sink point M_0. It is assumed that $D_0/H_0\ll 1$, $H_0/H_1\ll 1$ and $\tilde{k}=k_p/k_0\gg 1$. With these assumptions, the heat transfer direction in the k_0 material is approximately perpendicular to the surface of the disk-shaped high thermal conductivity material; the high thermal conductivity material is of isotropy, and the heat transfer direction in the disk-shaped k_p material radially points to the center of the disk. The volume $V_{p,0}$ of k_p material ($V_{p,0}=\pi[D_1^2(H_0-D_0)+H_1^2D_0]/4$), i.e., the fraction of high thermal conductivity material $\phi_0=V_{p,0}/V_0$, is fixed, but the ratio D_1/D_0 is free to vary. The thermal current in the cylindrical element is continuous, and the peak temperature locates at the ring of diameter H_1 (point P_0), which is situated the farthest from the heat sink (M_0).

One way to assemble a number of (n) cylindrical elements to form the first order assembly is shown in Figure 2 [21]. The thermal current from the centre of the disk-shaped k_p material is collected by the cylindrical high conductivity channel (diameter D_1, length L_1, and thermal conductivity coefficient k_p) of the first order assembly. Finally, the thermal current flows to the heat sink located at point M_1. The boundary of the first order assembly is adiabatic except for the heat sink point M_1. The volume of the first order assembly V_1 (diameter H_1, length L_1, $V_1=nV_0=\pi H_1^2L_1/4$) is fixed, but the ratios D_1/D_0, H_0/H_1 and the number of the cylindrical elements n are free to vary. The volume of high thermal conductivity material $V_{p,1}$ ($V_{p,1}=n\pi H_1^2D_0/4+n\pi D_1^2\times(H_0-D_0)/4$), i.e., the fraction of high thermal conductivity material $\phi_1=V_{p,1}/V_1$, is fixed.

3.2 Heat conduction model with rectangular element on microscale and nanoscale

A rectangular element ($H_0\times L_0\times 1$) generates heat volumetrically (heat generation rate per unit volume is q''', and it is considered as a uniform internal heat source in the rectan-

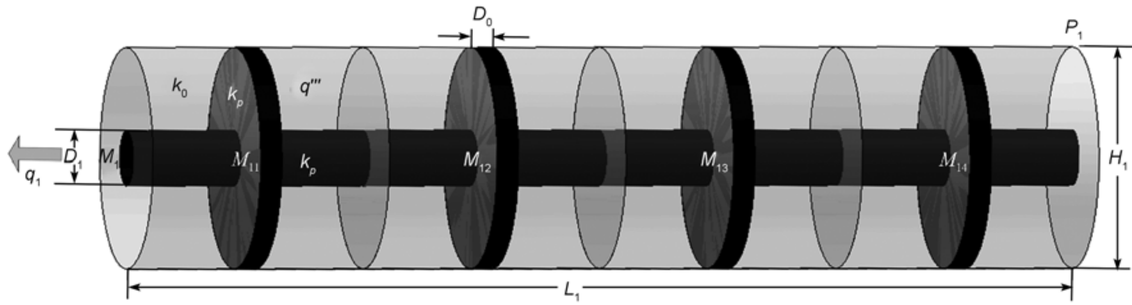

Figure 2 Cylindrical first order assembly [21].

gular element) as shown in Figure 3. The elemental area size A_0 is constant, but the ratio H_0/L_0 is free to vary. The heat generated in the k_0 material is first collected by a high conductivity channel (width D_0, thermal conductivity coefficient k_x, $k_x \gg k_0$) located on the longer axes of the rectangular element, and then flows to the heat sink located at point M_0 along the high conductivity channel. The boundary of the rectangular elemental area is adiabatic except for the heat sink point M_0. It is assumed that the area occupied by high conductive material is much smaller than that occupied by low conductivity material ($\phi_0 = D_0 / H_0 \ll 1$), and the rectangular element is slender enough ($H_0 \ll L_0$). With these assumptions, the heat transfer direction is approximately parallel to y-direction in the low conductivity material, and is parallel to x-direction in the high conductivity material.

When the width D_0 of the high conductivity channel reduces to microscale and nanoscale, the thermal conductivity coefficient of the high conductivity channel will change, which is caused by size effect. The model shown by eq. (6) in ref. [31] reflects the change of the thermal conductivity coefficient of the high conductivity channel due to size effect.

$$\frac{k_x}{k_b} = \begin{cases} \dfrac{D}{\lambda} & (D \leqslant \lambda), \\ 1 & (D > \lambda), \end{cases} \tag{6}$$

where λ is the dimension bound (10–100 nm), at which the size effect becomes significant in the high conductivity channel. When the width D is sufficiently large, the thermal conductivity coefficient of the high conductivity channel does not depend on D with a constant value k_b; when the width D is not bigger than λ, the size effect will take effect, and k_x is relative to the width D.

A large number n_1 of optimized rectangular elements are assembled into the first order assembly ($A_1 = H_1 \times L_1$) as it is shown in Figure 4 [31]. The rectangular elements (n_1) shown in Figure 3 are distributed on the both sides of the new high conductivity channel (width D_1, thermal conductivity k_x) shown in Figure 4. The elemental heat currents from the nodes $M_{11}, M_{12}, \ldots, M_{1,n_1/2}$ are collected by the new high conductivity channel, and the outer boundary of A_1 is adiabatic except for the D_1 patch over the origin M_1, through which the collected heat current is led to the outside. The shape of the first order assembly H_1/L_1 or the number of rectangular elements n_1 is free to vary. Similarly, a large number n_2 of optimized rectangular first order assemblies are assembled into the second order assembly ($A_2 = H_2 \times L_2$) as it is shown in Figure 5 [31]. The rectangular first order

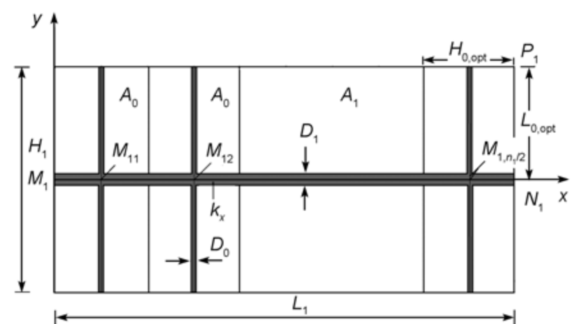

Figure 4 Rectangular first order assembly [31].

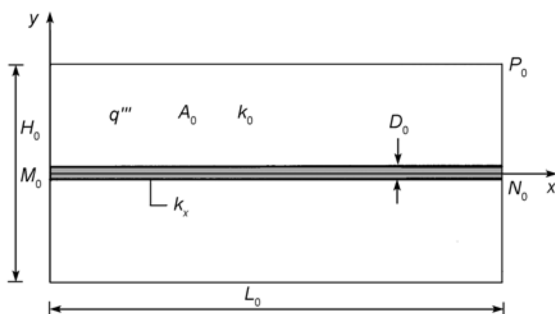

Figure 3 Rectangular element [31].

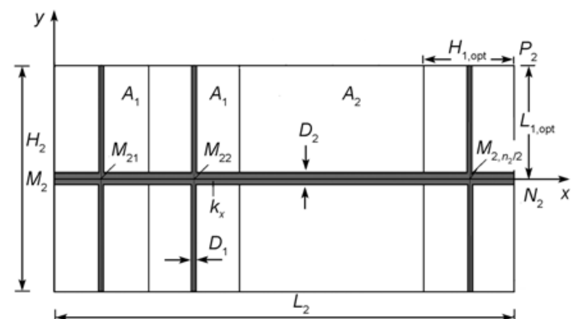

Figure 5 Rectangular second order assembly [31].

assemblies (n_2) shown in Figure 4 are distributed on the both sides of the new high conductivity channel (width D_2, thermal conductivity k_x shown in Figure 5. The shape of the second order assembly H_2/L_2 or the number of the rectangular first order assemblies n_2 is free to vary.

3.3 Heat conduction model with triangular element on microscale and nanoscale

A triangular element ($H_0 \times L_0 \times 1/2$) generates heat volumetrically (heat generation rate per unit volume is q''', and it is considered as a uniform internal heat source in the triangular element) and is shown in Figure 6 [13]. The elemental area size A_0 is constant, but the ratio H_0/L_0 is free to vary. The first order and second order assemblies are obtained by assembling the triangular elements as done in Section 3.2. The effect of size effect on the heat transfer performance of the triangular construct when the width of the high conductivity channel reduces to microscale and nanoscale is considered.

4 Constructal optimization of the three-dimensional cylindrical assembly

4.1 Optimization of the cylindrical element

As it is shown in Figure 1, according to the heat conduction differential equation of the cylindrical element, the temperature difference distribution in the low conductivity material and disc-shaped high conductivity channel is

$$T(x,r)-T_3\left(\frac{H_0}{2}\right)=\frac{q'''}{2k_0}\left(\frac{H_0^{\,2}}{4}-x^2\right)+\frac{q'''H_0}{2k_pD_0}\times\left[\frac{H_1^{\,2}}{4}\ln\left(\frac{2r}{D_1}\right)+\frac{D_1^{\,2}}{8}-\frac{r^2}{2}\right],$$
$$(0\leqslant x\leqslant H_0/2,\ D_1/2\leqslant r\leqslant H_1/2). \tag{7}$$

For the case $H_0/2\leqslant x\leqslant H_0$, the temperature difference can be obtained by replacing x with (H_0–x) in eq. (7).

From eqs. (4) and (7), the entransy dissipation rate in the low conductivity material and disc-shaped high conductivity channel is

$$\begin{aligned}\dot{E}_{vh\phi01}&=2\int_0^{2\pi}\int_0^{\frac{H_0}{2}}\int_{\frac{D_1}{2}}^{\frac{H_1}{2}}q'''\left\{\frac{q'''}{2k_0}\left(\frac{H_0^{\,2}}{4}-x^2\right)+\frac{q'''H_0}{2k_pD_0}\times\left[\frac{H_1^{\,2}}{4}\ln\left(\frac{2r}{D_1}\right)+\frac{D_1^{\,2}}{8}-\frac{r^2}{2}\right]\right\}r\mathrm{d}r\mathrm{d}x\mathrm{d}\theta\\&=\frac{\pi q'''^2H_0^{\,2}}{384D_0k_0k_p}[(H_1^{\,2}-D_1^{\,2})(3k_0D_1^{\,2}-9k_0H_1^{\,2}+8k_pD_0H_0)+12k_0H_1^{\,4}\ln\left(\frac{H_1}{D_1}\right)].\end{aligned}\tag{8}$$

The temperature difference distribution in the cylindrical high conductivity channel is

$$T_3(x)-T_3(0)=\frac{4q'''V_0x}{\pi D_1^{\,2}k_p}\quad(0\leqslant x\leqslant H_0/2). \tag{9}$$

From eqs. (4) and (9), the entransy dissipation rate in the cylindrical high conductivity channel is

$$\dot{E}_{vh\phi02}=\int_0^{\frac{H_0}{2}}k_p\left(\frac{\mathrm{d}T_3}{\mathrm{d}x}\right)^2\frac{\pi D_1^{\,2}}{4}\mathrm{d}x=\frac{2q'''^2V_0^{\,2}H_0}{\pi k_pD_1^{\,2}}. \tag{10}$$

From eqs. (8) and (10), the entransy dissipation rate in the cylindrical element becomes

$$\begin{aligned}\dot{E}_{vh\phi0}&=\dot{E}_{vh\phi01}+\dot{E}_{vh\phi02}=2H_0q'''^2V_0^{\,2}/(\pi k_pD_1^{\,2})+\pi q'''^2\\&\quad\times H_0^{\,2}[(H_1^{\,2}-D_1^{\,2})(3D_1^{\,2}k_0-9H_1^{\,2}k_0+8k_pD_0H_0)\\&\quad+12H_1^{\,4}k_0\ln(H_1/D_1)]/(384D_0k_0k_p).\end{aligned}\tag{11}$$

The dimensionless variables are defined as follows:

$$\tilde{H}_0,\tilde{D}_0,\tilde{H}_1,\tilde{D}_1=\frac{H_0,D_0,H_1,D_1}{V_0^{\,1/3}}. \tag{12}$$

The volume constraints of the first order assembly and high thermal conductivity material can be nondimensionalized as

$$\frac{\pi\tilde{H}_1^{\,2}\tilde{H}_0}{4}=1, \tag{13}$$

$$\phi_0=\frac{\tilde{D}_0}{4}\left[2\cdot(2\pi)^{1/3}\left(\frac{\tilde{H}_0}{\tilde{H}_1}\right)^{-2/3}-\pi\tilde{D}_0^{\,2}\left(\frac{\tilde{D}_1}{\tilde{D}_0}\right)^2+(2\pi)^{2/3}\tilde{D}_0\left(\frac{\tilde{H}_0}{\tilde{H}_1}\right)^{2/3}\left(\frac{\tilde{D}_1}{\tilde{D}_0}\right)^2\right]. \tag{14}$$

According to eqs. (5), (11) and (13), the dimensionless equivalent thermal resistance of the cylindrical element is

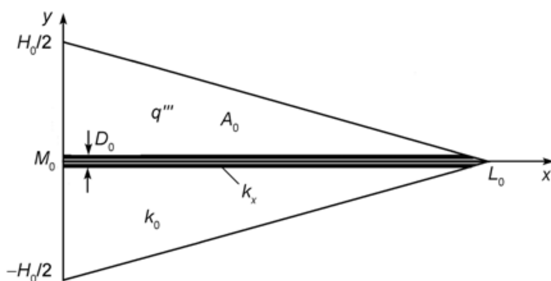

Figure 6 Triangular element [13].

$$
\begin{aligned}
\tilde{R}_{h0} &= \frac{\dot{E}_{vh\phi 0}}{\dot{Q}_{h0}^{\,2}/(k_0 V_0^{1/3})} \\
&= \left\{ -72\pi^{1/3}\tilde{D}_0 \left(\frac{\tilde{D}_1}{\tilde{D}_0}\right)^2 - 16\pi^{4/3}\tilde{k}\tilde{D}_0^{\,4}\left(\frac{\tilde{H}_0}{\tilde{H}_1}\right)^2 \right. \\
&\quad \times \left(\frac{\tilde{D}_1}{\tilde{D}_0}\right)^4 + 2^{1/3}\pi^{2/3}\tilde{D}_0^{\,2}\left(\frac{\tilde{H}_0}{\tilde{H}_1}\right)^{4/3}\left(\frac{\tilde{D}_1}{\tilde{D}_0}\right)^2 \\
&\quad \times \left[32\tilde{k} - 3\pi\tilde{D}_0^{\,3}\left(\frac{\tilde{D}_1}{\tilde{D}_0}\right)^4\right] + 24\cdot 2^{2/3}\left(\frac{\tilde{H}_0}{\tilde{H}_1}\right)^{2/3} \\
&\quad \times \left[16 + \pi\tilde{D}_0^{\,3}\left(\frac{\tilde{D}_1}{\tilde{D}_0}\right)^4\right] + 96\pi^{1/3}\tilde{D}_0\left(\frac{\tilde{D}_1}{\tilde{D}_0}\right)^2 \\
&\quad \left. \times \ln\left[2^{2/3}(\pi^{1/3}\tilde{D}_0)^{-1}\left(\frac{\tilde{H}_0}{\tilde{H}_1}\right)^{-1/3}\left(\frac{\tilde{D}_1}{\tilde{D}_0}\right)^{-1}\right]\right\} \\
&\quad \times \left[192\pi^{4/3}\tilde{k}\tilde{D}_0^{\,2}\left(\frac{\tilde{D}_1}{\tilde{D}_0}\right)^2\right]^{-1},
\end{aligned}
\tag{15}
$$

where $\tilde{D}_0$ is determined by eq. (14). The function $\tilde{R}_{h0}$ has two degrees of freedom for the fixed $\tilde{k}$ and ϕ_0, and one can use H_0/H_1 and D_1/D_0 as two degrees of freedom to carry out constructal optimization for the cylindrical element.

Figure 7 shows the dimensionless equivalent thermal resistance $\tilde{R}_{h0}$ versus H_0/H_1 characteristic with $\tilde{k}=300$, ϕ_0=0.1 and different D_1/D_0. From Figure 7, there exists an optimal H_0/H_1 ($(H_0/H_1)_{\rm opt}$) which leads to minimum $\tilde{R}_{h0}$ ($\tilde{R}_{h0,\rm m}$); with the increase in D_1/D_0, $\tilde{R}_{h0,\rm m}$ decreases first, and then increases.

Figure 8 shows $\tilde{R}_{h0,\rm m}$ and $(H_0/H_1)_{\rm opt}$ versus D_1/D_0 characteristics with $\tilde{k}=300$ and ϕ_0=0.1. From Figure 8, $(H_0/H_1)_{\rm opt}$ decreases with the increase in D_1/D_0; there exist optimal D_1/D_0 ($(D_1/D_0)_{\rm opt}$) and $(H_0/H_1)_{\rm opt}$ ($(H_0/H_1)_{\rm oo}$) which lead to double minimum $\tilde{R}_{h0}$ ($\tilde{R}_{h0,\rm mm}$).

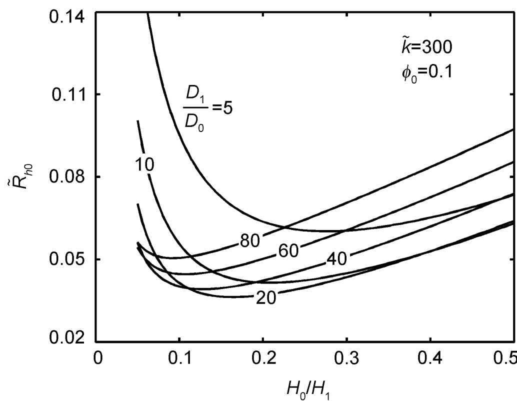

Figure 7 $\tilde{R}_{h0}$ versus H_0/H_1 characteristic with different D_1/D_0.

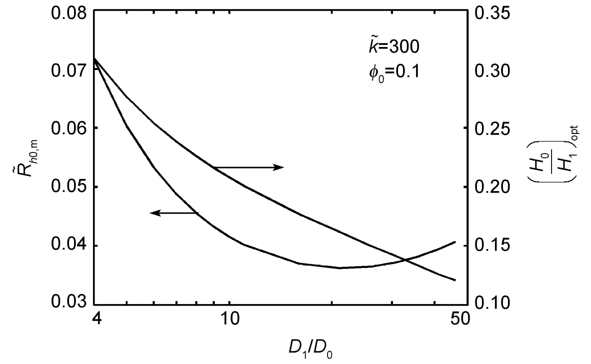

Figure 8 $\tilde{R}_{h0,\rm m}$ and $(H_0/H_1)_{\rm opt}$ versus D_1/D_0 characteristics.

4.2 Optimization of the cylindrical first order assembly

As shown in Figure 2, according to the method of calculating entransy dissipation rate in ref. [53], the entransy dissipation rate along D_1 channel is calculated by the sum of entransy dissipation rates of all intervals M_1, M_{11}, M_{12}, $\dots, M_{1n}$ on the D_1 channel, and is given as follows:

$$
\begin{aligned}
\dot{E}_{h\phi,M_{1,n}M_1} &= \dot{E}_{h\phi,M_{11}M_1} + \sum_{j=2}^{n}\dot{E}_{h\phi,M_{1,j}M_{1,j-1}} \\
&= \frac{(nq'''V_0)^2 H_0}{k_p\pi D_1^2/2} + \sum_{j=2}^{n}\frac{(q'''V_0)^2[n-(j-1)]^2 H_0}{k_p\pi D_1^2/4} \\
&= \frac{2H_0(q'''V_1)^2}{3k_p\pi D_1^2}\left(2n+\frac{1}{n}\right),\quad n\geqslant 2.
\end{aligned}
\tag{16}
$$

According to eqs. (8) and (16), the entransy dissipation rate of the cylindrical first order assembly is

$$
\begin{aligned}
\dot{E}_{vh\phi 1} &= n\dot{E}_{vh\phi 01} + \dot{E}_{h\phi,M_{1,n}M_1} \\
&= q'''^2 H_0\{256V_1^2(1/n+2n)/D_1^2 \\
&\quad + \pi^2 nH_0[(H_1^2-D_1^2)(3k_0D_1^2-9k_0H_1^2 \\
&\quad + 8k_pD_0H_0) + 12H_1^4 k_0\ln(H_1/D_1)] \\
&\quad \times (k_0D_0)^{-1}\}/(384\pi k_p),
\end{aligned}
\tag{17}
$$

The dimensionless variables are defined as follows:

$$
\tilde{H}_0, \tilde{D}_0, \tilde{H}_1, \tilde{L}_1, \tilde{D}_1 = \frac{H_0, D_0, H_1, L_1, D_1}{V_1^{1/3}}. \tag{18}
$$

The volume constraints of the cylindrical first order assembly and high thermal conductivity material can be nondimensionalized as

$$
\frac{\pi\tilde{H}_1^{\,2}\tilde{L}_1}{4} = 1, \tag{19}
$$

$$\phi_1 = \frac{\tilde{D}_0}{4}\left[2\cdot(2\pi)^{1/3} n^{-2/3}\left(\frac{\tilde{H}_0}{\tilde{H}_1}\right)^{-2/3} - \pi\tilde{D}_0^{\,2}\left(\frac{\tilde{D}_1}{\tilde{D}_0}\right)^2 + (2\pi)^{2/3}\tilde{D}_0 n^{-1/3}\left(\frac{\tilde{H}_0}{\tilde{H}_1}\right)^{2/3}\left(\frac{\tilde{D}_1}{\tilde{D}_0}\right)^2 \right]. \tag{20}$$

According to eqs. (5), (17) and (19), the dimensionless equivalent thermal resistance of the cylindrical first order assembly is

$$\begin{aligned}\tilde{R}_{h1} &= \frac{\dot{E}_{vh\phi 1}}{\dot{Q}_{h1}^2/(k_0 V_1^{1/3})} \\ &= \left\{ (2\pi n)^{2/3}\tilde{D}_0^{\,2}\left(\frac{\tilde{H}_0}{\tilde{H}_1}\right)^{4/3}\left(\frac{\tilde{D}_1}{\tilde{D}_0}\right)^2 \right. \\ &\times\left[32k - 3\pi n\times\tilde{D}_0^3\left(\frac{\tilde{D}_1}{\tilde{D}_0}\right)^4\right] - 72(2\pi n)^{1/3}\tilde{D}_0\left(\frac{\tilde{D}_1}{\tilde{D}_0}\right)^2 \\ &- 16\cdot 2^{1/3}\times(\pi n)^{4/3}\tilde{k}\tilde{D}_0^{\,4}\left(\frac{\tilde{H}_0}{\tilde{H}_1}\right)^2\left(\frac{\tilde{D}_1}{\tilde{D}_0}\right)^4 + 16\left(\frac{\tilde{H}_0}{\tilde{H}_1}\right)^{2/3} \\ &\times\left[16 + 32n^2 + 3n\pi\tilde{D}_0^3\left(\frac{\tilde{D}_1}{\tilde{D}_0}\right)^4\right] + 96(2\pi n)^{1/3}\tilde{D}_0 \\ &\left.\times\left(\frac{\tilde{D}_1}{\tilde{D}_0}\right)^2 \ln\left[2^{2/3}(n\pi)^{-1/3}\tilde{D}_0^{-1}\left(\frac{\tilde{H}_0}{\tilde{H}_1}\right)^{-1/3}\times\left(\frac{\tilde{D}_1}{\tilde{D}_0}\right)^{-1}\right]\right\} \Bigg/ \\ &\left[192\cdot 2^{1/3}(\pi n)^{4/3}\tilde{k}\tilde{D}_0^{\,2}\left(\frac{\tilde{D}_1}{\tilde{D}_0}\right)^2\right],\end{aligned} \tag{21}$$

where $\tilde{D}_0$ is determined by eq. (20). The function $\tilde{R}_{h1}$ has two degrees of freedom for the fixed $\tilde{k}$, ϕ_1 and n, and one can use H_0/H_1 and D_1/D_0 as two degrees of freedom to carry out constructal optimization for the cylindrical first order assembly.

Figures 9–11 show the effects of the cylindrical elemental number n on heat transfer performance and optimal construct of the first order assembly with different $\tilde{k}$ and ϕ_1. From Figure 9, $\tilde{R}_{h1,\mathrm{mm}}$ decreases with the increase in $\tilde{k}$ and ϕ_1 for the fixed n; when n>5, the decrement of $\tilde{R}_{h1,\mathrm{mm}}$ becomes small, and the improvement of the heat transfer performance of the cylindrical first order assembly is not obvious. From Figures 10 and 11, with the increase in n, $(D_1/D_0)_{\mathrm{opt}}$ increases, $(H_0/H_1)_{\mathrm{oo}}$ decreases, and the D_1 channel becomes smaller, the disc-shaped high thermal conductivity material becomes thinner, and the first order assembly becomes slenderer; the effects of the cylindrical elemental number n on the internal aspect ratio $(D_1/D_0)_{\mathrm{opt}}$ and external aspect ratio $(L_1/H_1)_{\mathrm{oo}}$ $(n\cdot(H_0/H_1)_{\mathrm{oo}})$ are more sensitive than those of $\tilde{k}$ and ϕ_1.

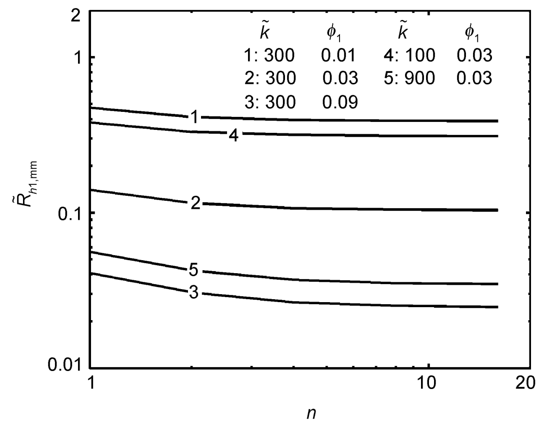

Figure 9 Effect of n on $\tilde{R}_{h1,\mathrm{mm}}$ with different $\tilde{k}$ and ϕ_1.

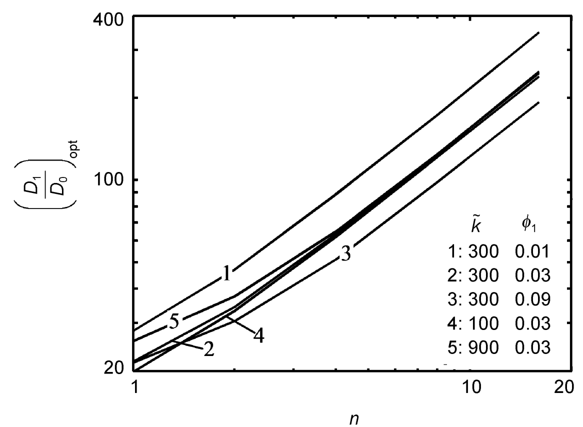

Figure 10 Effect of n on $(D_1/D_0)_{\mathrm{opt}}$ with different $\tilde{k}$ and ϕ_1.

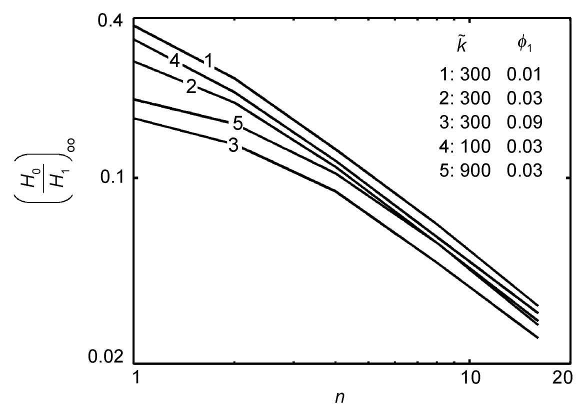

Figure 11 Effect of n on $(H_0/H_1)_{\mathrm{oo}}$ with different $\tilde{k}$ and ϕ_1.

Table 1 lists the optimal constructs of the cylindrical first order assembly based on the minimizations of dimensionless equivalent thermal resistance and dimensionless maximum thermal resistance ($\tilde{R}_{t1} = T_{P1}/(q''' V_1^{2/3}/k_0)$) with ϕ_1=0.01, $\tilde{k}=300$ and different n. Table 1 shows that the optimal constructs of the cylindrical first order assemblies

Table 1 Optimal constructs of the cylindrical first order assembly based on the minimizations of dimensionless equivalent thermal resistance and dimensionless maximum thermal resistance

Element number	Minimum dimensionless equivalent thermal resistance			Minimum dimensionless maximum thermal resistance		
n	$\tilde{R}_{h1,\mathrm{mm}}$	$(D_1/D_0)_{\mathrm{opt}}$	$(H_0/H_1)_{\mathrm{opt}}$	$\tilde{R}_{t1,\mathrm{mm}}$	$(D_1/D_0)_{\mathrm{opt}}$	$(H_0/H_1)_{\mathrm{opt}}$
1	0.0362	21.7	0.1599	0.0468	19.8	0.1477
2	0.0269	30.4	0.1294	0.0356	29.9	0.1170
4	0.0230	51.3	0.0851	0.0309	52.3	0.0762
8	0.0217	96.9	0.0473	0.0294	99.9	0.0422
16	0.0214	190.6	0.0244	0.0290	197.3	0.0217
32	0.0213	379.6	0.0123	0.0288	393.8	0.0109

based on the minimizations of dimensionless equivalent thermal resistance and dimensionless maximum thermal resistance are different. The $(H_0/H_1)_{\mathrm{opt}}$ based on dimensionless equivalent thermal resistance minimization is always larger than that based on dimensionless maximum thermal resistance minimization, that is, the construct of the three-dimensional cylindrical first order assembly based on the dimensionless equivalent thermal resistance minimization is slenderer than that based on the dimensionless maximum thermal resistance minimization. The minimization of maximum thermal resistance chases for the minimum maximum temperature difference of the construct, and can effectively reduce its maximum temperature limitation; the minimization of dimensionless equivalent thermal resistance chases for the temperature gradient homogenization of the construct, and can improve its global heat transfer performance, which are the main reason for the difference of the optimal constructs based on the minimizations of these two objectives.

For the fixed thermal current $((q'''V_1))$ of the cylindrical first order assembly, the average temperature difference of the cylindrical first order assembly is proportional to its equivalent thermal resistance. Numerical calculations show that comparing the dimensionless equivalent thermal resistance (the average temperature difference) based on minimum entransy dissipation rate with that based on minimum maximum temperature difference, the decrement of the dimensionless equivalent thermal resistance is relevant to $\tilde{k}$, ϕ_1 and n. When $\tilde{k}=1000$, $\phi_1=0.25$ and $n=2$, the dimensionless equivalent thermal resistance based on minimum entransy dissipation rate decreases by 2.01% compared with that based on minimum maximum temperature difference. However, according to the comparison results of the two-dimensional rectangular first order assemblies based on the minimizations of equivalent thermal resistance and maximum thermal resistance, the optimal constructs assembling by the optimal rectangular elements in refs. [10, 53] as well as those assembling by the unconfined rectangular elements in refs. [12, 54] are the same. At this point, by comparing the equivalent thermal resistance based on minimum entransy dissipation rate with that based on minimum maximum temperature difference, the equivalent thermal resistance is not reduced any more, which is obviously different from the comparison between the constructs of the three-dimensional cylindrical first order assembly based on the minimizations of these two objectives.

5 Constructal optimization of the rectangular assembly on microscale and nanoscale

5.1 Optimization of the rectangular element on microscale and nanoscale

In the rectangular element as shown in Figure 3, when the width of the high conductivity channel reduces to microscale and nanoscale and considering the case $D_0 \leqslant \lambda$, the thermal conductivity coefficient of the high conductivity channel D_0 under the size effect becomes $k_x = k_b D_0/\lambda$. For the case $y>0$, according to ref. [31], the temperature difference distribution of the rectangular element in Figure 3 can be described as

$$\Delta T_0(x,y)=\frac{q'''}{2k_0}\left(H_0 y-y^2\right)+\frac{q'''\tilde{\lambda}}{k_b\phi_0^2}\left(\frac{H_0}{L_0}\right)^{-1/2}\left(L_0 x-\frac{x^2}{2}\right), \quad (22)$$

where $\tilde{\lambda}=\lambda/A_0^{1/2}$. For the case $y<0$, the temperature difference can be obtained by replacing H_0 with $-H_0$ in eq. (22).

According to eqs. (4) and (5), the entransy dissipation rate and dimensionless equivalent thermal resistance of the rectangular element are, respectively, given by

$$\dot{E}_{vh\phi 0}=2\int_0^{\frac{H_0}{2}}\int_0^{L_0} q'''\left[\frac{q'''}{2k_0}\left(H_0 y-y^2\right)+\frac{q'''\tilde{\lambda}_0}{k_b\phi_0^2}\left(\frac{H_0}{L_0}\right)^{-1/2}\left(L_0 x-\frac{x^2}{2}\right)\right]\mathrm{d}x\mathrm{d}y, \quad (23)$$

$$\tilde{R}_{h0}=\frac{\dot{E}_{vh\phi 0}}{q'''^2 A_0^2/k_0}=\frac{H_0}{12L_0}+\frac{\tilde{\lambda}}{3\tilde{k}\phi_0^2}\left(\frac{H_0}{L_0}\right)^{-3/2}, \quad (24)$$

where $\tilde{k} = k_b / k_0$. $\tilde{R}_{h0}$ is minimized with respect to the aspect ratio H_0/L_0 of the rectangular element, and the corresponding optimization results are

$$\left(H_0 / L_0\right)_{\text{opt}}^{\text{n}} = \left(\frac{6\tilde{\lambda}}{\tilde{k}\phi_0^{\ 2}}\right)^{2/5}, \tag{25}$$

$$\tilde{R}_{h0,\text{m}}^{\text{n}} = \frac{5}{6^{8/5}}\left(\frac{\tilde{\lambda}}{\tilde{k}\phi_0^{\ 2}}\right)^{2/5}, \tag{26}$$

where the superscript "n" indicates that these results are obtained when the size effect takes effect in the high conductivity channel.

When $D_0 \leqslant \lambda$, i.e. $\tilde{\lambda} \geqslant \tilde{\lambda}_{c,0}$ ($\tilde{\lambda}_{c,0} = \phi_0 (H_0 / L_0)^{1/2}$), eqs. (25) and (26) are valid. To evaluate the value of $\tilde{\lambda}_{c,0}$, substituting eq. (25) into the expression of $\tilde{\lambda}_{c,0}$ and replacing $\tilde{\lambda}$ by $\tilde{\lambda}_{c,0}$, the magnitude order of $\tilde{\lambda}_{c,0}$ becomes [31]

$$\tilde{\lambda}_{c,0} \sim \frac{6^{1/4}\phi_0^{\ 3/4}}{\tilde{k}^{1/4}}. \tag{27}$$

Eq. (27) indicates the order of magnitude of $\tilde{\lambda}_{c,0}$.

When $D_0 > \lambda$, the size effect is not present in the high conductivity channel with a constant thermal conductivity coefficient k_b. The optimal shape and the corresponding minimum dimensionless equivalent thermal resistance of the rectangular element are, respectively, given by [53]

$$\left(H_0 / L_0\right)_{\text{opt}}^{\text{b}} = \frac{2}{(\tilde{k}\phi_0)^{1/2}}, \tag{28}$$

$$\tilde{R}_{h0,\text{m}}^{\text{b}} = \frac{1}{3(\tilde{k}\phi_0)^{1/2}}, \tag{29}$$

where the superscript "b" indicates that these results are obtained when the size effect is not present in the high conductivity channel when D_0/λ.

Figures 12 and 13 show the effects ϕ_0 on the characteristics of $\tilde{R}_{h0,\text{m}}$ and $(H_0/L_0)_{\text{opt}}$ versus $\tilde{\lambda}$, respectively. When $\tilde{\lambda} \geqslant \tilde{\lambda}_{c,0}$, eqs. (25) and (26) are the optimal constructs of the rectangular element based on dimensionless equivalent thermal resistance minimization, i.e., the lines marked "n" shown in Figures 12 and 13; when $\tilde{\lambda} < \tilde{\lambda}_{c,0}$, eqs. (28) and (29) are the optimal construct of the rectangular element based on dimensionless equivalent thermal resistance minimization, i.e., the lines marked "b" shown in Figures 12 and 13. From Figures 12 and 13, because of the effect of the size effect on the high conductivity channel, the minimum dimensionless equivalent thermal resistance of the rectangular element $\tilde{R}_{h0,\text{m}}$ increases with the increase in $\tilde{\lambda}$, and the optimal shape of the rectangular element becomes tubbier.

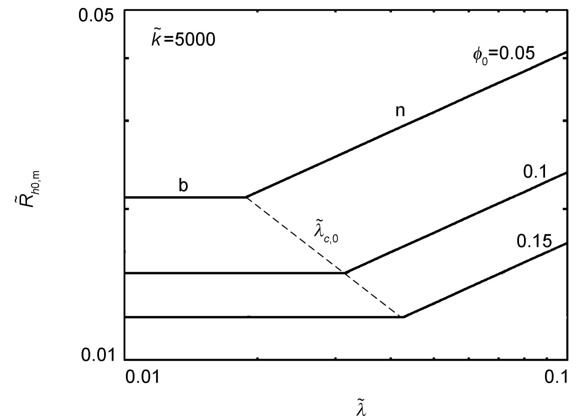

Figure 12 Effect ϕ_0 on the characteristic of $\tilde{R}_{h0,\text{m}}$ versus $\tilde{\lambda}$.

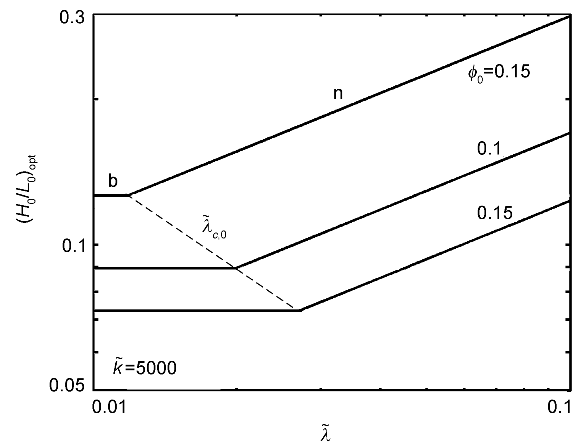

Figure 13 Effect ϕ_0 on the characteristic of $(H_0/L_0)_{\text{opt}}$ versus $\tilde{\lambda}$.

5.2 Optimization of the rectangular first order assembly on microscale and nanoscale

As it is shown in Figure 4, when the volume fraction of high conductivity material in the first order assembly ϕ_1 ($\phi_1 = (n_1 L_0 D_0 + D_1 L_1) / A_1$) is fixed, one has $D_1 = H_1 \times (\phi_1 - \phi_0)$. When the width D_1 of the high conductivity channel reduces to microscale and nanoscale, and considering the case $D_1 \leqslant \lambda$, the thermal conductivity coefficient of the high conductivity channel D_1 under the size effect becomes $k_x = k_b D_1 / \lambda$. According to the different widths of the high conductivity channels D_0 and D_1, there are three conduction regimes in the first order assembly due to the size effects on the high conductivity channels [31]: when $D_0 \leqslant \lambda$ and $D_1 \leqslant \lambda$, the notation "nn" indicates that the size effect takes effect both in channels D_0 and D_1; when $D_0 \leqslant \lambda$ and $D_1 > \lambda$, the notation "nb" indicates that the size effect takes effect only in channel D_0, and does not in channel D_1; when $D_0 > \lambda$ and $D_1 > \lambda$, the notation "bb" indicates that the size effect

does not takes effect in both channels D_0 and D_1.

When $D_0 \leqslant \lambda$ and $D_1 \leqslant \lambda$, the entransy dissipation rate along D_1 channel is calculated by the sum of entransy dissipation rates of all intervals $M_1, M_{11}, M_{12}, \ldots, M_{1n}$ on the D_1 channel. When $n_1 \gg 1$, it is reasonable to assume that the distribution of the thermal current density along D_1 is linear. According to eq. (3) and ref. [53], the entransy dissipation rate along D_1 channel is

$$\dot{E}_{h\phi, M_{1,n_1/2}M_1} = \int_0^{L_1} q'''H_1 \cdot \frac{q'''H_1\tilde{\lambda}A_0^{1/2}(L_1x - x^2/2)}{k_b D_1^2}\mathrm{d}x = \frac{q'''^2 A_0^{5/2} H_0 \tilde{\lambda} n_1^3}{6 k_b D_1^2}, \quad n_1 \geqslant 2, \tag{30}$$

where n_1 is an even.

The entransy dissipation rate of the first order assembly is the sum of the entransy dissipation rate in each element and D_1 channel. From eqs. (26) and (30), the dimensionless equivalent thermal resistance of the first order assembly is

$$\tilde{R}_{h1} = \frac{\dot{E}_{vh\phi 1}}{q'''^2 A_1^2/k_0} = \frac{n_1\dot{E}_{vh\phi 0} + \dot{E}_{h\phi, M_{1,n_1/2}M_1}}{q'''^2 A_1^2/k_0} = \frac{n_1(\tilde{\lambda}/\tilde{k})^{8/5}}{4\cdot 6^{2/5}\phi_0^{6/5}(\phi_1-\phi_0)^2} + \frac{5}{6\cdot 6^{3/5} n_1}\cdot\left(\frac{\tilde{\lambda}}{\tilde{k}\phi_0^2}\right)^{2/5}. \tag{31}$$

Similarly, for the cases of "nb" and "bb", $\tilde{R}_{h1}$ also can be derived. Furthermore, $\tilde{R}_{h1}$ can be optimized with respect to the number of elements n_1 and the volume fraction of high conductivity material in the rectangular element ϕ_0, and the corresponding optimal constructs of the first order assembly are listed in Table 2.

When the distribution of the thermal current density along high conductivity channel is linear with the length, the optimal constructs of the rectangular first order assemblies based on the minimizations of entransy dissipation rate (listed in Table 2) and maximum temperature difference in ref. [31] are the same.

When $\tilde{\lambda} > \tilde{\lambda}_{c,1}$ ($\tilde{\lambda}_{c,1} A_0^{1/2} \sim D_{1,\mathrm{opt}}^{\mathrm{nn}}$), from the optimization result of $\tilde{R}_{h1}^{\mathrm{nn}}$, $D_{1,\mathrm{opt}}^{\mathrm{nn}} = (\tilde{k}\phi_1^7/\tilde{\lambda})^{1/5} A_0^{1/2}/(2^{3/5}\cdot 3^{1/5})$, one has [31]

$$\tilde{\lambda}_{c,1} \sim \frac{\tilde{k}^{1/6}\phi_1^{7/6}}{2^{1/2}\cdot 3^{1/6}}. \tag{32}$$

Eq. (32) indicates the order of magnitude of $\tilde{\lambda}_{c,1}$.

Figure 14 shows the effects ϕ_1 on the minimum dimensionless equivalent thermal resistance of the first order assembly $\tilde{R}_{h1,\mathrm{mm}}$ versus $\tilde{\lambda}$ characteristic. When $\tilde{\lambda} \geqslant \tilde{\lambda}_{c,1}$, $\tilde{R}_{h1,\mathrm{mm}}$ is represented by the lines marked "nn" shown in Figure 14; when $\tilde{\lambda}_{c,0} \leqslant \tilde{\lambda} < \tilde{\lambda}_{c,1}$, $\tilde{R}_{h1,\mathrm{mm}}$ is represented by the lines marked "nb" shown in Figure 14; when $\tilde{\lambda} < \tilde{\lambda}_{c,0}$, $\tilde{R}_{h1,\mathrm{mm}}$ is represented by the lines marked "bb" shown in Figure 14. From Figure 14, because of the effect of the size effect on channels D_0 and D_1, with the increase in $\tilde{\lambda}$, $\tilde{R}_{h1,\mathrm{mm}}$ increases.

Suppose the volume of each assembly and the volume fraction of high conductivity material in each assembly are the same, that is, $\phi_0=\phi_1=\phi$ and $A_0=A_1=A$. Comparing $\tilde{R}_{h0,\mathrm{m}}^{\mathrm{n}}$ and $\tilde{R}_{h1,\mathrm{mm}}^{\mathrm{nn}}$, when $\tilde{k}\phi^2/\tilde{\lambda} < 15.8165$, the minimum dimensionless equivalent thermal resistance of the elemental design (the structure form is n) is smaller than that of the first order design (the structure form is nn), and the elemental design should be adopted; while when $\tilde{k}\phi^2/\tilde{\lambda} > 15.8165$, the conclusion is reversed. Comparing $\tilde{R}_{h0,\mathrm{m}}^{\mathrm{n}}$ and $\tilde{R}_{h1,\mathrm{mm}}^{\mathrm{nb}}$, when $\tilde{k}\phi < 13.5691$ the minimum dimensionless equivalent thermal resistance of the elemental design (the structure form is n) is smaller than that of the first order design (the structure form is nb), and the elemental design should be adopted; while when $\tilde{k}\phi > 13.5691$, the conclusion is reversed.

Table 2 Optimal constructs of the rectangular first order assembly with three structure forms based on entransy dissipation rate minimization

Structure form	$n_{1,\mathrm{opt}}$	$\phi_{0,\mathrm{opt}}$	$\left(\frac{D_1}{D_0}\right)_{\mathrm{opt}}$	$\left(\frac{H_1}{L_1}\right)_{\mathrm{opt}}$	$\tilde{R}_{h1,\mathrm{mm}}$
nn	$\frac{5^{1/2}}{2^{4/5}\cdot 3^{3/5}}\cdot\left(\frac{\tilde{k}\phi_1^2}{\tilde{\lambda}}\right)^{3/5}$	$\frac{\phi_1}{2}$	$\frac{(\tilde{k}\phi_1^2/\tilde{\lambda})^{2/5}}{2^{1/5}\cdot 3^{2/5}}$	$\frac{2^{8/5}\cdot 3^{1/5}}{5^{1/2}}\left(\frac{\tilde{\lambda}}{\tilde{k}\phi_1^2}\right)^{1/5}$	$\frac{2\sqrt{5}\tilde{\lambda}}{3\tilde{k}\phi_1^2}$
nb	$5\sqrt{\frac{\tilde{k}\phi_1}{39}}$	$\frac{8\phi_1}{13}$	$\frac{5}{3^{2/5}\cdot 13^{4/5}}\left(\frac{\tilde{k}\phi_1^2}{\tilde{\lambda}}\right)^{2/5}$	$\frac{16\cdot 3^{1/10}}{5\cdot 13^{3/10}}\left(\frac{\phi_1^3}{\tilde{k}\tilde{\lambda}^4}\right)^{1/10}$	$\frac{13^{13/10}\tilde{\lambda}^{2/5}}{24\cdot 3^{1/10}(\tilde{k}^9\phi_1^{13})^{1/10}}$
bb	$\sqrt{\tilde{k}\phi_1}$	$\frac{\phi_1}{2}$	$\left(\frac{\tilde{k}\phi_1}{2}\right)^{1/2}$	$\sqrt{2}$	$\frac{2^{3/2}}{3\tilde{k}\phi_1}$

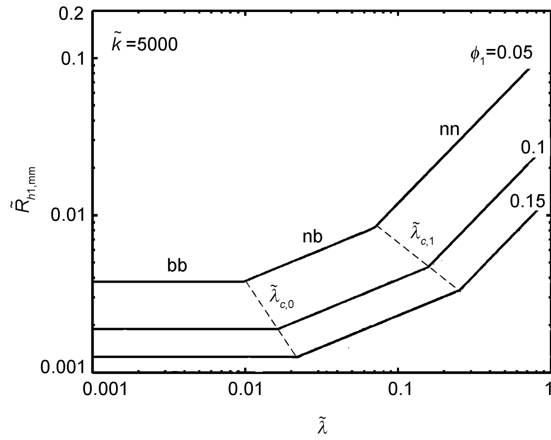

Figure 14 Effect ϕ_1 on the characteristic of $\tilde{R}_{h1,\mathrm{mm}}$ versus $\tilde{\lambda}$.

5.3 Optimization of the rectangular second order assembly on microscale and nanoscale

As it is shown in Figure 5, when the volume fraction of high conductivity material in the second order assembly ϕ_2 ($\phi_2=(n_1\phi_1 A_1+D_2L_2)/A_2$) is fixed, one has $D_2=H_2\times(\phi_2-\phi_1)$. According to the different widths of high conductivity channels D_0, D_1 and D_2, there are four conduction regimes in the second order assembly due to the size effects on the high conductivity channels: nnn, nnb, nbb and bbb [31]. When $D_0\leqslant\lambda$, $D_1\leqslant\lambda$ and $D_2\leqslant\lambda$, the notation "nnn" indicates that the size effect takes effect in channels D_0, D_1 and D_2; when $D_0\leqslant\lambda$, $D_1\leqslant\lambda$ and $D_2>\lambda$, the notation "nnb" indicates that the size effect takes effect in both channels D_0 and D_1, and but does not in channel D_2; when $D_0\leqslant\lambda$, $D_1>\lambda$ and $D_2>\lambda$, the notation "nbb" indicates that the size effect takes effect in channel D_0, and does not in channels D_1 and D_2; when $D_0>\lambda$, $D_1>\lambda$ and $D_2>\lambda$, the notation "bbb" indicates that the size effect does not take effect in channels D_0, D_1 and D_2. Similar to the optimization method of the first order assembly, the dimensionless equivalent thermal resistance of the rectangular second order assembly can be optimized, and the corresponding optimal constructs of the second order assemblies are listed in Table 3.

$$\begin{aligned}&6\cdot 3^{1/5}(\tilde{k}\tilde{\lambda}^3)^{6/5}(\phi^{\mathrm{nnn}}_{1,\mathrm{opt}})^{24/5}(8\phi^{\mathrm{nnn}}_{1,\mathrm{opt}}-3\phi_2)\\&+5^{3/2}\cdot 2^{1/5}\cdot 3^{3/5}\tilde{k}^{9/5}\tilde{\lambda}^3(\phi^{\mathrm{nnn}}_{1,\mathrm{opt}})^4(29\phi^{\mathrm{nnn}}_{1,\mathrm{opt}}\\&-14\phi_2)(\phi_2-\phi^{\mathrm{nnn}}_{1,\mathrm{opt}})^2+125\cdot 2^{2/5}\tilde{k}^{8/5}(\tilde{k}\tilde{\lambda}^3)^{4/5}\\&\times(\phi^{\mathrm{nnn}}_{1,\mathrm{opt}})^{16/5}(13\phi^{\mathrm{nnn}}_{1,\mathrm{opt}}-8\phi_2)(\phi_2-\phi^{\mathrm{nnn}}_{1,\mathrm{opt}})^4=0,\end{aligned}\tag{33}$$

$$\begin{aligned}\tilde{R}^{\mathrm{nnn}}_{h2,\mathrm{mm}}=&\tilde{\lambda}\{3[\tilde{k}\tilde{\lambda}^3(\phi^{\mathrm{nnn}}_{1,\mathrm{opt}})^4]^{1/5}[2+(n^{\mathrm{nnn}}_{2,\mathrm{opt}})^2]\\&+10\cdot 2^{1/5}\cdot 3^{2/5}\cdot 5^{1/2}\tilde{k}^{4/5}(\phi_2-\phi^{\mathrm{nnn}}_{1,\mathrm{opt}})^2\}\\&\times[15\cdot 2^{1/5}\cdot 3^{2/5}\tilde{k}^{9/5}n^{\mathrm{nnn}}_{2,\mathrm{opt}}(\phi^{\mathrm{nnn}}_{1,\mathrm{opt}})^2(\phi_2-\phi^{\mathrm{nnn}}_{1,\mathrm{opt}})^2]^{-1},\end{aligned}\tag{34}$$

$$\begin{aligned}&2\cdot 3^{2/5}(\phi^{\mathrm{nnb}}_{1,\mathrm{opt}})^{16/5}(7\phi^{\mathrm{nnb}}_{1,\mathrm{opt}}-2\phi_2)+5\cdot 2^{2/5}\cdot 3^{1/5}\\&\times(\phi^{\mathrm{nnb}}_{1,\mathrm{opt}})^{8/5}(\tilde{k}\tilde{\lambda}^4)^{1/5}(31\phi^{\mathrm{nnb}}_{1,\mathrm{opt}}-16\phi_2)(\phi_2-\phi^{\mathrm{nnb}}_{1,\mathrm{opt}})\\&+25\cdot 2^{4/5}(\tilde{k}\tilde{\lambda}^4)^{2/5}(17\phi^{\mathrm{nnb}}_{1,\mathrm{opt}}-12\phi_2)(\phi_2-\phi^{\mathrm{nnb}}_{1,\mathrm{opt}})^2=0,\end{aligned}\tag{35}$$

$$\begin{aligned}\tilde{R}^{\mathrm{nnb}}_{h2,\mathrm{mm}}=&\tilde{\lambda}^{1/5}\{10\cdot 2^{2/5}(\tilde{k}\tilde{\lambda}^4)^{1/5}(\phi_2-\phi^{\mathrm{nnb}}_{1,\mathrm{opt}})\\&+3^{1/5}[2+(n^{\mathrm{nnb}}_{2,\mathrm{opt}})^2](\phi^{\mathrm{nnb}}_{1,\mathrm{opt}})^{8/5}\}/[3\cdot 2^{2/5}\\&\times 5^{1/2}\tilde{k}^{6/5}n^{\mathrm{nnb}}_{2,\mathrm{opt}}(\phi^{\mathrm{nnb}}_{1,\mathrm{opt}})^2(\phi_2-\phi^{\mathrm{nnb}}_{1,\mathrm{opt}})],\end{aligned}\tag{36}$$

$$\begin{aligned}&274625\cdot 13^{1/5}\tilde{k}^{2/5}\tilde{\lambda}^{8/5}(\phi_2-\phi^{\mathrm{nbb}}_{1,\mathrm{opt}})^2(2\phi^{\mathrm{nbb}}_{1,\mathrm{opt}}-\phi_2)\\&+64\cdot 3^{1/5}\{448\cdot 3^{1/5}(\phi^{\mathrm{nbb}}_{1,\mathrm{opt}})^{21/5}+192\cdot 3^{1/5}\phi_2\\&\times(\phi^{\mathrm{nbb}}_{1,\mathrm{opt}})^{16/5}-65\cdot 13^{3/5}(\tilde{k}\tilde{\lambda}^4)^{1/5}(\phi^{\mathrm{nbb}}_{1,\mathrm{opt}})^{8/5}\\&\times[17(\phi^{\mathrm{nbb}}_{1,\mathrm{opt}})^2-19\phi^{\mathrm{nbb}}_{1,\mathrm{opt}}\phi_2+2{\phi_2}^2]\}=0,\end{aligned}\tag{37}$$

$$\begin{aligned}\tilde{R}^{\mathrm{nbb}}_{h2,\mathrm{mm}}=&\{32\cdot 3^{1/5}\tilde{k}^{4/5}(\phi^{\mathrm{nbb}}_{1,\mathrm{opt}})^{8/5}[2+(n^{\mathrm{nbb}}_{2,\mathrm{opt}})^2]\\&+65\cdot 13^{3/5}\tilde{k}\tilde{\lambda}^{4/5}(\phi_2-\phi^{\mathrm{nbb}}_{1,\mathrm{opt}})\}/[120\cdot 3^{1/10}\\&\times 13^{3/10}\tilde{k}^{19/10}\tilde{\lambda}^{2/5}n^{\mathrm{nbb}}_{2,\mathrm{opt}}(\phi^{\mathrm{nbb}}_{1,\mathrm{opt}})^{13/10}(\phi_2-\phi^{\mathrm{nbb}}_{1,\mathrm{opt}})].\end{aligned}\tag{38}$$

Table 3 Optimal constructs of the rectangular second order assembly with four structure forms based on entransy dissipation rate minimization

Structure form	nnn	nnb	nbb	bbb
$n_{2,\mathrm{opt}}$	$\{2+2^{6/5}\cdot 5^{3/2}\tilde{k}^{3/5}(\phi_2-\phi^{\mathrm{nnn}}_{1,\mathrm{opt}})^2\times[3^{3/5}\tilde{\lambda}^{3/5}(\phi^{\mathrm{nnn}}_{1,\mathrm{opt}})^{4/5}]^{-1}\}^{1/2}$	$\{2+10\cdot 2^{2/5}(\tilde{k}\tilde{\lambda}^4)^{1/5}(\phi_2-\phi^{\mathrm{nnb}}_{1,\mathrm{opt}})/[3^{1/5}(\phi^{\mathrm{nnb}}_{1,\mathrm{opt}})^{8/5}]\}^{1/2}$	$\{2+65\cdot 3^{4/5}\cdot 13^{3/5}(\tilde{k}\tilde{\lambda}^4)^{1/5}(\phi_2-\phi^{\mathrm{nbb}}_{1,\mathrm{opt}})/[96(\phi^{\mathrm{nbb}}_{1,\mathrm{opt}})^{8/5}]\}^{1/2}$	2
$\phi_{1,\mathrm{opt}}$	eq. (33)	eq. (35)	eq. (37)	$0.6202\phi_2$
$\left(\dfrac{D_2}{D_1}\right)_{\mathrm{opt}}$	$\dfrac{2^{2/5}\cdot 5^{1/2}(\phi_2-\phi^{\mathrm{nnn}}_{1,\mathrm{opt}})}{3^{1/5}(\phi^{\mathrm{nnn}}_{1,\mathrm{opt}})^{3/5}}\left(\dfrac{\tilde{k}}{\tilde{\lambda}}\right)^{1/5}$	$\dfrac{2^{2/5}\cdot 5^{1/2}(\phi_2-\phi^{\mathrm{nnb}}_{1,\mathrm{opt}})}{3^{1/5}(\phi^{\mathrm{nnb}}_{1,\mathrm{opt}})^{3/5}}\left(\dfrac{\tilde{k}}{\tilde{\lambda}}\right)^{1/5}$	$\dfrac{13^{13/10}}{8\cdot 3^{1/10}}\cdot\dfrac{\tilde{\lambda}^{2/5}\tilde{k}^{1/10}(\phi_2-\phi^{\mathrm{nbb}}_{1,\mathrm{opt}})}{(\phi^{\mathrm{nbb}}_{1,\mathrm{opt}})^{13/10}}$	3.4641
$\left(\dfrac{H_2}{L_2}\right)_{\mathrm{opt}}$	$\dfrac{2^{2/5}\cdot 5^{1/2}(\phi^{\mathrm{nnn}}_{1,\mathrm{opt}})^{2/5}}{3^{1/5}n^{\mathrm{nnn}}_{2,\mathrm{opt}}}\left(\dfrac{\tilde{k}}{\tilde{\lambda}}\right)^{1/5}$	$\dfrac{2^{2/5}\cdot 5^{1/2}(\phi^{\mathrm{nnb}}_{1,\mathrm{opt}})^{2/5}}{3^{1/5}n^{\mathrm{nnb}}_{2,\mathrm{opt}}}\left(\dfrac{\tilde{k}}{\tilde{\lambda}}\right)^{1/5}$	$\dfrac{5\cdot 13^{3/10}}{4\cdot 3^{1/10}}\cdot\dfrac{\tilde{\lambda}^{2/5}\tilde{k}^{1/10}}{n^{\mathrm{nbb}}_{2,\mathrm{opt}}(\phi^{\mathrm{nbb}}_{1,\mathrm{opt}})^{3/10}}$	$\sqrt{2}$
$\tilde{R}_{h2,\mathrm{mm}}$	eq. (34)	eq. (36)	eq. (38)	$\dfrac{1.2255}{\tilde{k}\phi_2}$

Figure 15 shows the effect ϕ_2 on the minimum dimensionless equivalent thermal resistance of the second order assembly $\tilde{R}_{h2,\rm mm}$ versus $\tilde{\lambda}$ characteristic. When $\tilde{\lambda} \geqslant \tilde{\lambda}_{c,2}$, $\tilde{R}_{h2,\rm mm}$ is represented by the lines marked "nnn" shown in Figure 15; when $\tilde{\lambda}_{c,0} \leqslant \tilde{\lambda} < \tilde{\lambda}_{c,1}$, $\tilde{R}_{h2,\rm mm}$ is represented by the lines marked "nnb" shown in Figure 15; when $\tilde{\lambda} < \tilde{\lambda}_{c,0}$, $\tilde{R}_{h2,\rm mm}$ is represented by the lines marked "bbb" shown in Figure 15. From Figure 15, because of the effect of the size effect on channels D_0, D_1 and D_2, $\tilde{R}_{h2,\rm mm}$ increases with the increase in $\tilde{\lambda}$.

To compare the optimal constructs of the rectangular second order assembly based on the minimizations of entransy dissipation rate and maximum temperature difference [31], the structure form nbb of the rectangular second order assembly is taken as an example in the analysis. When $\tilde{k} = 5000$, ϕ_2=0.01 and $\tilde{\lambda} = 0.03$, From Table 3, the optimal number of the optimized first order assemblies is $n_{2,\rm opt}$=4.77 based on minimum entransy dissipation rate. $n_{2,\rm opt}$ should be an even number actually, and it may be 4 or 6; according to ref. [31], the optimal number of the optimized first order assemblies is $n_{2,\rm opt}$=3.90 based on minimum maximum temperature difference, and it may be 2 or 4. Noting that the length of the D_2 channel is not equal to L_2 [7, 53], the expression of width D_2 varies with n_2. When n_2=2, $D_2 = 2H_2(\phi_2 - \phi_1)$; when n_2=4, $D_2 = 4H_2(\phi_2 - \phi_1)/3$; when n_2=6, $D_2 = 6H_2(\phi_2 - \phi_1)/5$. For the fixed $n_{2,\rm opt}$, both $\tilde{R}_{h2}$ and $\tilde{R}_{t2}$ ($\tilde{R}_{t2} = \Delta T_{2,\max} \times (q'''A_2/k_0)^{-1}$) can be re-optimized with respect to ϕ_1, and the corresponding optimization results are listed in Table 4.

From Table 4, the optimal number of the optimized first order assemblies $n_{2,\rm opt}$ in rectangular second order assembly is small, and the distribution of the thermal current density along D_2 channel is no long linear with the length, the

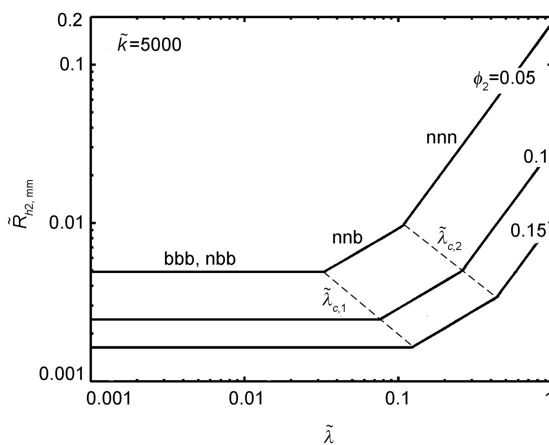

Figure 15 Effect ϕ_2 on the characteristic of $\tilde{R}_{h2,\rm mm}$ versus $\tilde{\lambda}$.

Table 4 Optimal constructs of the rectangular second order assembly when the structure form is nbb

Optimization objective	Entransy dissipation rate minimization	Maximum temperature difference minimization[a)]
$n_{2,\rm opt}$	4	2
$\left(\frac{D_2}{D_1}\right)_{\rm opt}$	5.5490	2.9833
$\left(\frac{H_2}{L_2}\right)_{\rm opt}$	0.8485	1.5297
$\tilde{R}_{h2}$	0.002795	0.003021
$\tilde{R}_{t2}$	0.003965	0.003933

a) This row is deduced by the authors according to ref. [31].

optimal constructs of the rectangular second order assemblies based on the minimizations of entransy dissipation rate and maximum temperature difference [31] are different. Comparing the optimization result based on the entransy dissipation rate minimization with that based on the maximum temperature difference minimization, $n_{2,\rm opt}$ is unequal, the shape of the rectangular second order assembly is slenderer, and the width ratio of the channels D_2 and D_1 is bigger. For the fixed thermal current ($(q'''A_2 \times 1)$) of the rectangular second order assembly, the average temperature difference of the rectangular second order assembly is proportional to its equivalent thermal resistance. The dimensionless equivalent thermal resistance (the average temperature difference) based on minimum entransy dissipation rate decreases by 7.48% compared with that based on minimum maximum temperature difference; but the dimensionless maximum thermal resistance (maximum temperature difference) based on minimum entransy dissipation rate only increases by 0.81% compared with that based on minimum maximum temperature difference. Thus, the optimal construct based on minimum entransy dissipation rate can more effectively reduce the average temperature difference of the rectangular assembly than that based on minimum maximum temperature difference, and its heat transfer performance improves simultaneously.

6 Constructal optimization of the triangular assembly on microscale and nanoscale

According to ref. [13], the temperature difference distribution of the triangular element (y>0) in Figure 6 can be given as follows:

$$\Delta T_0(x,y) = \frac{q'''}{2k_0}\left[H_0 y\left(1-\frac{x}{L_0}\right) - y^2\right] + \frac{2\sqrt{2}q'''\tilde{\lambda}}{k_b\phi_0^2}\left(\frac{H_0}{L_0}\right)^{-1/2}\left(\frac{L_0 x}{2} - \frac{x^2}{2} + \frac{x^3}{6L_0}\right), \quad (39)$$

where $\tilde{\lambda} = \lambda / A_0^{1/2}$. For the case y<0, the temperature difference can be obtained by replacing H_0 with $-H_0$ in eq. (39).

According to eqs. (4), (5) and (39), the entransy dissipation rate and dimensionless equivalent thermal resistance of the triangular element are, respectively, given by

$$\dot{E}_{vh\phi 0} = 2\int_0^{L_0}\int_0^{\frac{H_0}{2}\left(1-\frac{x}{L_0}\right)} q'''\left[\frac{q'''}{2k_0}\left[H_0 y\left(1-\frac{x}{L_0}\right)-y^2\right] + \frac{2\sqrt{2}q'''\tilde{\lambda}}{k_b\phi_0^2}\left(\frac{H_0}{L_0}\right)^{-1/2}\left(\frac{L_0 x}{2}-\frac{x^2}{2}+\frac{x^3}{6L_0}\right)\right]\mathrm{d}y\mathrm{d}x, \quad (40)$$

$$\tilde{R}_{h0} = \frac{\dot{E}_{vh\phi 0}}{q'''^2 A_0^2 / k_0} = \frac{H_0}{12L_0} + \frac{2\sqrt{2}\tilde{\lambda}}{5\tilde{k}\phi_0^2}\left(\frac{H_0}{L_0}\right)^{-3/2}. \quad (41)$$

Similar to the optimization method in Section 5, the dimensionless equivalent thermal resistance of the triangular element as well as first order and second order assemblies can be optimized, and the corresponding optimal constructs of each assembly are listed in Tables 5–7.

$$10\cdot 6^{3/10}\tilde{k}^3\tilde{\lambda}^{3/5}(\phi_{1,\mathrm{opt}}^{\mathrm{nnn}})^{4/5}(29\phi_{1,\mathrm{opt}}^{\mathrm{nnn}}-14\phi_2)(\phi_2-\phi_{1,\mathrm{opt}}^{\mathrm{nnn}})^2 +5\cdot 30^{3/5}\tilde{k}^{18/5}(13\phi_{1,\mathrm{opt}}^{\mathrm{nnn}}-8\phi_2)(\phi_2-\phi_{1,\mathrm{opt}}^{\mathrm{nnn}})^4+8\cdot 5^{2/5} \times[\tilde{k}^{12}\tilde{\lambda}^6(\phi_{1,\mathrm{opt}}^{\mathrm{nnn}})^8]^{1/5}(8\phi_{1,\mathrm{opt}}^{\mathrm{nnn}}-3\phi_2)=0, \quad (42)$$

$$\tilde{R}_{h2,\mathrm{mm}}^{\mathrm{nnn}} = 2^{11/5}\left(\frac{\tilde{\lambda}}{\tilde{k}}\right)^{8/5}\left\{5^{2/5}[2+(n_{2,\mathrm{opt}}^{\mathrm{nnn}})^2] \times(\phi_{1,\mathrm{opt}}^{\mathrm{nnn}})^{4/5}+5\cdot 6^{3/10}\left(\frac{\tilde{k}}{\tilde{\lambda}}\right)^{3/5}(\phi_2-\phi_{1,\mathrm{opt}}^{\mathrm{nnn}})^2\right\} \times[5\cdot 3^{4/5}n_{2,\mathrm{opt}}^{\mathrm{nnn}}(\phi_{1,\mathrm{opt}}^{\mathrm{nnn}})^2(\phi_2-\phi_{1,\mathrm{opt}}^{\mathrm{nnn}})^2]^{-1}, \quad (43)$$

$$2^{2/5}\cdot 5^{1/5}\{3^{4/5}\cdot 5^{3/5}[\tilde{k}^4(\phi_{1,\mathrm{opt}}^{\mathrm{nnb}})^{48}\tilde{\lambda}^{-4}]^{1/5}(7\phi_{1,\mathrm{opt}}^{\mathrm{nnb}}-2\phi_2) +45\cdot 2^{1/5}(17\phi_{1,\mathrm{opt}}^{\mathrm{nnb}}-12\phi_2)(\phi_2-\phi_{1,\mathrm{opt}}^{\mathrm{nnb}})^2[\tilde{k}^6\tilde{\lambda}^4(\phi_{1,\mathrm{opt}}^{\mathrm{nnb}})^{32}]^{1/5}\} -15\cdot 3^{2/5}\tilde{k}(\phi_{1,\mathrm{opt}}^{\mathrm{nnb}})^8[31(\phi_{1,\mathrm{opt}}^{\mathrm{nnb}})^2-47\phi_{1,\mathrm{opt}}^{\mathrm{nnb}}\phi_2+16\phi_2^2]=0, \quad (44)$$

$$\tilde{R}_{h2,\mathrm{mm}}^{\mathrm{nnb}} = 2^{9/10}\{[2+(n_{2,\mathrm{opt}}^{\mathrm{nnb}})^2][\tilde{\lambda}(\phi_{1,\mathrm{opt}}^{\mathrm{nnb}})^8/\tilde{k}]^{1/5}+2\cdot 5^{1/5}\cdot 6^{3/5} \times\tilde{\lambda}(\phi_2-\phi_{1,\mathrm{opt}}^{\mathrm{nnb}})\}/[3^{11/10}\cdot 5^{1/5}n_{2,\mathrm{opt}}^{\mathrm{nnb}}\tilde{k}\phi_1^2(\phi_2-\phi_{1,\mathrm{opt}}^{\mathrm{nnb}})], \quad (45)$$

$$32\cdot 955\cdot 10^{2/5}\cdot 39^{3/5}(\tilde{k}\tilde{\lambda}^4)^{2/5}(\phi_2-\phi_{1,\mathrm{opt}}^{\mathrm{nbb}})^2(2\phi_{1,\mathrm{opt}}^{\mathrm{nbb}}-\phi_2) +64\{64\cdot 39^{2/5}(\phi_{1,\mathrm{opt}}^{\mathrm{nbb}})^{16/5}(3\phi_2+7\phi_{1,\mathrm{opt}}^{\mathrm{nbb}})-507\cdot 10^{1/5}[\tilde{k}\tilde{\lambda}^4 \times(\phi_{1,\mathrm{opt}}^{\mathrm{nbb}})^8]^{1/5}[17(\phi_{1,\mathrm{opt}}^{\mathrm{nbb}})^2-19\phi_{1,\mathrm{opt}}^{\mathrm{nbb}}\phi_2+2\phi_2^2]\}=0, \quad (46)$$

$$\tilde{R}_{h2,\mathrm{mm}}^{\mathrm{nbb}} = \{32\tilde{k}^{4/5}[2+(n_{2,\mathrm{opt}}^{\mathrm{nbb}})^2](\phi_{1,\mathrm{opt}}^{\mathrm{nbb}})^{8/5}+13\cdot 10^{1/5} \times 39^{3/5}\tilde{k}\tilde{\lambda}^{4/5}(\phi_2-\phi_{1,\mathrm{opt}}^{\mathrm{nbb}})\}/[12\cdot 2^{1/10}\cdot 5^{3/5} \times 39^{3/10}\tilde{k}^{19/10}\tilde{\lambda}^{2/5}(\phi_{1,\mathrm{opt}}^{\mathrm{nbb}})^{13/10}n_{2,\mathrm{opt}}^{\mathrm{nbb}}(\phi_2-\phi_{1,\mathrm{opt}}^{\mathrm{nbb}})]. \quad (47)$$

Table 5 Optimal constructs of the triangular element based on entransy dissipation rate minimization

Structure form	$\left(\frac{H_0}{L_0}\right)_{\mathrm{opt}}$	$\tilde{R}_{h0,\mathrm{m}}$
n	$\frac{2\cdot 3^{4/5}}{5^{2/5}}\left(\frac{\tilde{\lambda}}{\tilde{k}\phi_0^2}\right)^{2/5}$	$\frac{5^{3/5}}{6\cdot 3^{1/5}}\left(\frac{\tilde{\lambda}}{\tilde{k}\phi_0^2}\right)^{2/5}$
b	$2\sqrt{\frac{6}{5\tilde{k}\phi_0}}$	$\sqrt{\frac{2}{15\tilde{k}\phi_0}}$

Table 6 Optimal constructs of the triangular first order assembly based on entransy dissipation rate minimization

Structure form	nn	nb	bb
$n_{1,\mathrm{opt}}$	$\frac{5^{3/5}}{2\cdot 6^{7/10}}\left(\frac{\tilde{k}\phi_1^2}{\tilde{\lambda}}\right)^{3/5}$	$5\sqrt{\frac{\tilde{k}\phi_1}{78}}$	$\sqrt{\frac{\tilde{k}\phi_1}{2}}$
$\phi_{0,\mathrm{opt}}$	$\frac{\phi_1}{2}$	$\frac{8\phi_1}{13}$	$\frac{\phi_1}{2}$
$\left(\frac{D_1}{D_0}\right)_{\mathrm{opt}}$	$\frac{5^{2/5}}{2\cdot 6^{4/5}}\left(\frac{\tilde{k}\phi_1^2}{\tilde{\lambda}}\right)^{2/5}$	$\frac{5^{7/5}}{2^{3/5}\cdot 39^{4/5}}\left(\frac{\tilde{k}\phi_1^2}{\tilde{\lambda}}\right)^{2/5}$	$\frac{1}{2}\sqrt{\frac{5\tilde{k}\phi_1}{3}}$
$\left(\frac{H_1}{L_1}\right)_{\mathrm{opt}}$	$\frac{2^{19/10}}{3^{1/10}\cdot 5^{1/5}}\left(\frac{\tilde{\lambda}}{\tilde{k}\phi_1^2}\right)^{1/5}$	$\frac{8\cdot 2^{9/10}}{5^{3/5}\cdot 39^{3/10}}\left(\frac{\phi_1^3}{\tilde{k}\tilde{\lambda}^4}\right)^{1/10}$	$\sqrt{\frac{10}{3}}$
$\tilde{R}_{h1,\mathrm{mm}}$	$4\sqrt{\frac{2}{3}}\frac{\tilde{\lambda}}{\tilde{k}\phi_1^2}$	$\frac{13^{13/10}}{2^{19/10}\cdot 3^{7/10}\cdot 5^{2/5}}\frac{\tilde{\lambda}^{2/5}}{(\tilde{k}^9\phi_1^{13})^{1/10}}$	$4\sqrt{\frac{2}{15}}\frac{1}{\tilde{k}\phi_1}$

Table 7 Optimal constructs of the triangular second order assembly based on entransy dissipation rate minimization

Structure form	nnn	nnb	nbb	bbb
$n_{2,\mathrm{opt}}$	$[2+5^{3/5}\cdot 6^{3/10}\tilde{k}^{3/5}(\phi_2-\phi_{1,\mathrm{opt}}^{\mathrm{nnn}})^2 \times\tilde{\lambda}^{-3/5}(\phi_{1,\mathrm{opt}}^{\mathrm{nnn}})^{-4/5}]^{1/2}$	$[2+2\cdot 5^{1/5}\cdot 6^{3/5}(\phi_2-\phi_{1,\mathrm{opt}}^{\mathrm{nnb}}) \times(\tilde{k}\tilde{\lambda}^4)^{1/5}(\phi_{1,\mathrm{opt}}^{\mathrm{nnb}})^{-8/5}]^{1/2}$	$\{2+13\cdot 10^{1/5}\cdot 39^{3/5}(\tilde{k}\tilde{\lambda}^4)^{1/5} \times(\phi_2-\phi_{1,\mathrm{opt}}^{\mathrm{nbb}})/[32(\phi_{1,\mathrm{opt}}^{\mathrm{nbb}})^{8/5}]\}^{1/2}$	2
$\phi_{1,\mathrm{opt}}$	eq. (42)	eq. (44)	eq. (46)	$0.5585\phi_2$
$\left(\frac{D_2}{D_1}\right)_{\mathrm{opt}}$	$5^{1/5}\cdot 6^{1/10}\left[\frac{\tilde{k}}{\tilde{\lambda}(\phi_{1,\mathrm{opt}}^{\mathrm{nnn}})^3}\right]^{1/5}(\phi_2-\phi_{1,\mathrm{opt}}^{\mathrm{nnn}})$	$5^{1/5}\cdot 6^{1/10}\left[\frac{\tilde{k}}{\tilde{\lambda}(\phi_{1,\mathrm{opt}}^{\mathrm{nnb}})^3}\right]^{1/5}(\phi_2-\phi_{1,\mathrm{opt}}^{\mathrm{nnb}})$	$\frac{13\cdot 39^{3/10}\tilde{k}^{1/10}\tilde{\lambda}^{2/5}(\phi_2-\phi_{1,\mathrm{opt}}^{\mathrm{nbb}})}{4\cdot 2^{9/10}\cdot 5^{2/5}(\phi_{1,\mathrm{opt}}^{\mathrm{nbb}})^{13/10}}$	3.4641
$\left(\frac{H_2}{L_2}\right)_{\mathrm{opt}}$	$5^{1/5}\cdot 6^{1/10}\left[\frac{\tilde{k}(\phi_{1,\mathrm{opt}}^{\mathrm{nnn}})^2}{\tilde{\lambda}}\right]^{1/5}\Big/ n_{2,\mathrm{opt}}^{\mathrm{nnn}}$	$5^{1/5}\cdot 6^{1/10}\left[\frac{\tilde{k}(\phi_{1,\mathrm{opt}}^{\mathrm{nnb}})^2}{\tilde{\lambda}}\right]^{1/5}\Big/ n_{2,\mathrm{opt}}^{\mathrm{nnb}}$	$\frac{10^{3/5}\cdot 39^{3/10}\tilde{k}^{1/10}\tilde{\lambda}^{2/5}}{4\sqrt{2}(\phi_{1,\mathrm{opt}}^{\mathrm{nbb}})^{3/10}n_{2,\mathrm{opt}}^{\mathrm{nbb}}}$	1.0955
$\tilde{R}_{h2,\mathrm{mm}}$	eq. (43)	eq. (45)	eq. (47)	$\frac{2.3414}{\tilde{k}\phi_2}$

From Tables 5–7, the optimal constructs of the triangular element as well as the first order and second order assemblies based on minimization of dimensionless equivalent thermal resistance on microscale, nanoscale and convectional scale are obviously different. Because of the effect of the size effect on the thermal conductivity coefficient of the channel, with the increase in $\tilde{\lambda}$, the minimum dimensionless equivalent thermal resistance for each design method of each assembly increases.

To compare the optimal constructs of the triangular second order assembly based on the minimizations of entransy dissipation rate and maximum temperature difference, the structure form nnb of triangular second order assembly is taken as an example in the analysis. When $\tilde{k}=5000$, ϕ_2=0.01 and $\tilde{\lambda}=0.12$, from Table 7, the optimal number of the optimized first order assemblies is $n_{2,\mathrm{opt}}$=4.68 based on minimum entransy dissipation rate. $n_{2,\mathrm{opt}}$ should be an even number actually, and it may be 4 or 6; the optimal number of the optimized first order assemblies is $n_{2,\mathrm{opt}}$=3.30 based on minimum maximum temperature difference, and it may be 2 or 4. When n_2=2, $D_2=H_2(\phi_2-\phi_1)$; when n_2=4, $D_2=2H_2(\phi_2-\phi_1)/3$; when n_2=6, $D_2=3H_2(\phi_2-\phi_1)/5$. For the fixed $n_{2,\mathrm{opt}}$, both $\tilde{R}_{h2}$ and $\tilde{R}_{t2}$ ($\tilde{R}_{t2}=\Delta T_{2,\max}/(q'''A_2/k_0)$) can be re-optimized with respect to ϕ_1, and the corresponding optimization results are listed in Table 8.

From Table 8, the optimal constructs of triangular second order assembly based on the minimizations of entransy dissipation rate and maximum temperature difference are different. For the fixed thermal current $((q'''A_2\times 1))$ of the triangular second order assembly, the average temperature difference of the triangular second order assembly is proportional to its equivalent thermal resistance. The dimensionless equivalent thermal resistance (the average temperature difference) based on minimum entransy dissipation rate decreases by 11.03% compared with that based on minimum maximum temperature difference; but the dimensionless maximum thermal resistance (maximum temperature difference) based on minimum entransy dissipation rate only increases by 3.49% compared with that based on minimum maximum temperature difference. Thus, the optimal construct based on minimum entransy dissipation rate can more effectively reduce the mean temperature difference of the triangular assembly than that based on minimum maximum temperature difference, and its heat transfer performance improves simultaneously.

Table 8 Optimal constructs of the triangular second order assembly when the structure form is nnb

Optimization objective	Entransy dissipation rate minimization	Maximum temperature difference minimization
$n_{2,\mathrm{opt}}$	4	2
$\left(\frac{D_2}{D_1}\right)_{\mathrm{opt}}$	2.4636	1.7806
$\left(\frac{H_2}{L_2}\right)_{\mathrm{opt}}$	1.2117	2.2527
$\tilde{R}_{h2}$	0.007102	0.007983
$\tilde{R}_{t2}$	0.009288	0.008975

7 Conclusions

The three "volume-point" heat conduction models with three-dimensional cylindrical element and rectangular and triangular elements on microscale and nanoscale are studied respectively in this paper. The expressions of the dimensionless equivalent thermal resistances defined by entransy dissipation rate of these models are obtained. For the fixed volumes of each construct and high thermal conductivity material, the constructs of the three models are optimized by taking minimum entransy dissipation rate as optimization objective, and the optimal constructs of these models are obtained. The optimal results obtained by researching the model with three-dimensional cylindrical element show that the heat transfer performance of the cylindrical construct improves with the increase of $\tilde{k}$, ϕ_1 and n; however, when elemental number is big, the improvement of its heat transfer performance is not obvious. The effects of the elemental number on the internal aspect ratio $(D_1/D_0)_{\mathrm{opt}}$ and external aspect ratio $(L_1/H_1)_{\mathrm{oo}}$ are more sensitive than those of $\tilde{k}$ and ϕ_1. The constructs of three-dimensional cylindrical first order assembly based on the minimizations of dimensionless maximum thermal resistance and the dimensionless equivalent thermal resistance are different, which is obviously different from the comparison between the constructs of two-dimensional rectangular first order assembly based on the minimizations of these two objectives. The results obtained by researching the models with rectangular and triangular elements on microscale and nanoscale show that the optimal construct on microscale and nanoscale when the size effect takes effect is obviously different from that when the size effect does not take effect. With the increase in $\tilde{\lambda}$, the minimum dimensionless equivalent thermal resistance for each design method of each assembly increases. With the increase of the internal complexity of the construct, the dimensionless equivalent thermal resistance of the construct does not always decrease, and the different optimal internal design structures should be adopted according to different parameters. When the thermal current densities in the high conductivity channel are linear with the length, the optimal constructs of the element and first order assemblies based on the entransy dissipation rate minimization are the same as those based on the maximum temperature difference minimization in ref [31]; when the thermal current densities in the high conductivity channel are not linear ones, the optimal constructs of the second order assembly based on

the minimizations of these two objectives are different.

The entransy dissipation rate, associated with the entransy dissipation extremum principle, can provide a new objective for the optimization of heat transfer system, and can describe the global heat transfer ability of the system. The equivalent thermal resistance based on entransy dissipation rate minimization can reflect the average heat transfer performance of multi-dimensional heat conduction system, i.e., the smaller the equivalent thermal resistance, the lower the mean temperature difference of the construct, as well as the better heat transfer performance and the higher heat transfer efficiency of the construct. The constructal optimization work in this paper can provide an optimal alternative scheme from the point of view of heat transfer optimization for “volume-point” heat conduction models with three-dimensional cylindrical element and rectangular and triangular elements on microscale and nanoscale. The results obtained have enriched the constructal theory, and extended the application range of the entransy dissipation extremum principle.

This work was supported by the National Natural Science Foundation of China (Grant No. 51176203), the Natural Science Foundation of Naval University of Engineering (Grant No. HGDYDJJ10011) and the Natural Science Foundation for Youngsters of Naval University of Engineering (Grant No. HGDQNJJ10017). The authors wish to thank the three reviewers for their careful, unbiased and constructive suggestions, which led to this revised manuscript.

1 Bejan A. Shape and Structure, from Engineering to Nature. Cambridge: Cambridge University Press, 2000
2 Bejan A, Lorente S. Thermodynamic optimization of flow geometry in mechanical and civil engineering. J Non-Equilib Thermodyn, 2001, 26(4): 305–354
3 Bejan A, Lorente S. Constructal theory of generation of configuration in nature and engineering. J Appl Phys, 2006, 100(4): 041301
4 Bejan A, Merkx G W. Constructal Theory of Social Dynamics. New York: Springer, 2007
5 Bejan A, Lorente S. Design with Constructal Theory. New Jersey: Wiley, 2008
6 Bejan A, Lorente S, Miguel A F, et al. Constructal Human Dynamics, Security & Sustainability. Amsterdam: IOS Press, 2009
7 Bejan A. Constructal-theory network of conducting paths for cooling a heat generating volume, Trans ASME, J Heat Transfer, 1997, 40(4): 799–816
8 Ledezma G, Bejan A, Errera M. Constructal tree networks for heat transfer. J Appl Phys, 1997, 82(1): 89–100
9 Almogbel M, Bejan A. Constructal optimization of nonuniformly distributed tree-shaped flow structures for conduction. Int J Heat Mass Transfer, 2001, 44(22): 4185–4194
10 Ghodoossi L, Egrican N. Exact solution for cooling of electronics using constructal theory. J Appl Phys, 2003, 93(8), 4922–4929
11 Wu W, Chen L, Sun F. On the “area to point” flow problem based on constructal theory. Energy Convers Mgmt, 2007, 48(1): 101–105
12 Wu W, Chen L, Sun F. Improvement of tree-like network constructal method for heat conduction optimization. Sci China Ser-E: Tech Sci, 2006, 49(3): 332–341
13 Ghodoossi S, Egrican N. Conductive cooling of triangular shaped electronics using constructal theory. Energy Convers Mgmt, 2004, 45(6): 811–828
14 Wei S, Chen L, Sun F. The volume-point constructal optimization for discrete variable cross-section conducting path. Appl Energy, 2009, 86(7/8): 1111–1118
15 Zhou S, Chen L, Sun F. Optimization of constructal volume-point conduction with variable cross-section conducting path. Energy Convers Mgmt, 2007, 48(1): 106–111
16 Neagu M, Bejan A. Constructal-theory tree networks of ‘constant’ thermal resistance. J Appl Phys, 1999, 86(2): 1136–1144
17 Xiao Q, Chen L, Sun F. Constructal entransy dissipation rate minimization for heat conduction based on variable-shaped element. Chin Sci Bull, 2011, 56(22): 2400–2410
18 Karakas A, Camdali U, Tunc M. Constructal optimization of heat generating volumes. Int J Exergy, 2009, 6(5): 637–654
19 Ledezma G A, Bejan A. Constructal three-dimensional trees for conduction between a volume and one point. Trans ASME, J Heat Transfer, 1998, 120(4): 977–984
20 Neagu M, Bejan A. Three-dimensional tree constructs of ‘constant’ thermal resistance. J Appl Phys, 1999, 86(12): 7107–7115
21 Alebrahim A, Bejan A. Constructal trees of circular fins for conductive and convective heat transfer. Int J Heat Mass Transfer, 1999, 42(19): 3585–3597
22 Majumdar A. Microscale heat conduction in dielectric thin films. J Heat Transfer, 1993, 115, 7–16
23 Goodson K E, Flik M K. Electron and phonon thermal conduction in epitaxial high-Tc superconducting films. J Heat Transfer, 1993, 115, 17–25
24 Guo Z. Frontier of heat transfer–microscale heat transfer (in Chinese). Adv Mech, 2000, 30(1): 1–6
25 Duncan A B, Peterson G P. Review of microscale heat transfer. Appl Mech Rev, 1994, 47(9): 397–428
26 Gao P, Le Person S, Favre-Marinet M. Scale effects on hydrodynamics and heat transfer in two-dimensional mini and microchannels. Int J Therm Sci, 2002, 41(11), 1017–1027
27 Guo Z, Li Z. Size effect on microscale single-phase flow and heat transfer. Int J heat Mass Transfer, 2003, 46(1): 149–159
28 Guo Z, Li Z. Size effect on single-phase channel flow and heat transfer at microscale. Int J Heat Fluid Flow, 2003, 24(3), 284–298
29 Liu T, Ji J, Guo Z, et al. Achievements of major project "microscale heat transfer in astronautic technology and microeletronic devices" (in Chinese). Chin Sci fund, 2004, 6: 349–351
30 Hu X, Jain A, Goodson K E. Investigation of the natural convection boundary condition in microfabricated structures. Int J Therm Sci, 2008, 47(7): 820–824
31 Gosselin L, Bejan A. Constructal heat trees at micro and nanoscales. J Appl Phys, 2004, 96(10): 5852–5859
32 Guo Z, Zhu H, Liang X. Entransy -- A physical quantity describing heat transfer ability. Int J Heat Mass Transfer, 2007, 50(13/14): 2545–2556
33 Li Z, Guo Z. Field Synergy Principle of Heat Convection Optimization. Beijing: Science Press, 2010
34 Guo Z, Cheng X, Xia Z. Least dissipation principle of heat transport potential capacity and its application in heat conduction optimization. Chin Sci Bull, 2003, 48(4): 406–410
35 Han G, Zhu H, Cheng X, et al. Transfer similarity among heat conduction, elastic motion and electric conduction (in Chinese). J Eng Thermophys, 2005, 26(6): 1022–1024
36 Han G, Guo Z. Physical mechanism of heat conduction ability dissipation and its analytical expression (in Chinese). Proc CSEE, 2007, 27(17): 98–102
37 Zhu H, Chen J, Guo Z. Electricity and thermal analogous experimental study for entransy dissipation extreme principle (in Chinese). Prog Natural Sci, 2007, 17(12): 1692–1698
38 Chen Q, Ren J. Generalized thermal resistance for convective heat transfer and its relation to entransy dissipation. Chin Sci Bull, 2008, 53(23): 3753–3761
39 Chen Q, Ren J, Guo Z. The extremum principle of mass entransy dissipation and its application to decontamination ventilation designs in space station cabins. Chin Sci Bull, 2009, 54(16): 2862–2870
40 Xia S, Chen L, Sun F. Optimization for entransy dissipation minimi-

zation in heat exchanger. Chin Sci Bull, 2009, 54(19): 3587–3595
41 Wang S, Chen Q, Zhang B. An equation of entransy and its application. Chin Sci Bull, 2009, 54(19): 3572–3578
42 Guo J, Cheng L, Xu M. Entransy dissipation number and its application to heat exchanger performance evaluation. Chin Sci Bull, 2009, 54(15): 2708–2713
43 Chen Q, Wang M, Pan N, et al. Optimization principles for convective heat transfer. Energy, 2009, 34(9): 1199–1206
44 Chen L, Chen Q, Li Z, et al. Optimization for a heat exchanger couple based on the minimum thermal resistance principle. Int J Heat Mass Transfer, 2009, 52(21/22): 4778–4784
45 Guo Z, Liu X, Tao W, et al. Effectiveness-thermal resistance method for heat exchanger design and analysis. Int J Heat Mass Transfer, 2010, 53(13/14): 2877–2884
46 Xia S, Chen L, Sun F. Entransy dissipation minimization for liquid-solid phase processes. Sci China Tech Sci, 2010, 53(4): 960–968
47 Xia S, Chen L, Sun F. Entransy dissipation minimization for a class of one-way isothermal mass transfer processes. Sci China Tech Sci, 2011, 54(2): 352–361
48 Guo J, Xu M, Cheng L. Principle of equipartition of entransy dissipation for heat exchanger design. Sci China Tech Sci, 2010, 53(5): 1309–1314
49 Guo J, Xu M, Chen L. The influence of viscous heating on the entransy in two-fluid heat exchangers. Sci China: Tech Sci, 2011, 54(5): 1267–1274
50 Cheng X, Xu X, Liang X. Application of entransy to optimization design of parallel thermal network of thermal control system in spacecraft. Sci China Tech Sci, 2011, 54(4): 964–971
51 Cheng X, Liang X, Guo Z. Entransy decrease principle of heat transfer in an isolated system. Chin Sci Bull, 2011, 56(9): 847–854
52 Li X, Guo J, Xu M, et al. Entransy dissipation minimization for optimization of heat exchanger design. Chin Sci Bull, 2011, 56(20), 2174–2178
53 Wei S, Chen L, Sun F. "Volume-point" heat conduction constructal optimization with entransy dissipation minimization objective based on rectangular element. Sci China Ser E-Tech Sci, 2008, 51(8): 1283–1295
54 Wei S, Chen L, Sun F. Constructal entransy dissipation minimization for "volume-point" heat conduction without the premise of optimized last-order construct. Int J Exergy, 2010, 7(5): 627–639
55 Wei S, Chen L, Sun F. Constructal optimization of discrete and continuous-variable cross-section conducting path based on entransy dissipation rate minimization. Sci China Tech Sci, 2010, 53(6): 1666–1677
56 Wei S, Chen L, Sun F. "Volume-point" heat conduction constructal optimization with entransy dissipation minimization objective based on triangular element. Therm Sci, 2010, 14(4): 1075–1088
57 Wei S, Chen L, Sun F. Constructal multidisciplinary optimization of electromagnet based on entransy dissipation minimization. Sci China Ser E-Tech Sci, 2009, 52(10): 2981–2989
58 Xie Z, Chen L, Sun F. Constructal optimization for geometry of cavity by taking entransy dissipation minimization as objective. Sci China Ser E-Tech Sci, 2009, 52(12): 3504–3513
59 Xie Z, Chen L, Sun F. Constructal optimization on T-shaped cavity based on entransy dissipation minimization. Chin Sci Bull, 2009, 54(23): 4418–4427
60 Xiao Q Chen L, Sun F. Constructal entransy dissipation rate minimization for "disc-to-point" heat conduction. Chin Sci Bull, 2011, 56(1): 102–112
61 Chen L, Wei S, Sun F. Constructal entransy dissipation rate minimization of a disc. Int J Heat Mass Transfer, 2011, 54(1-3): 210–216
62 Xiao Q, Chen L, Sun F. Constructal entransy dissipation rate minimization for umbrella-shaped assembly of cylindrical fins. Sci China Tech Sci, 2011, 54(1): 211–219
63 Xie Z, Chen L, Sun F. Comparative study on constructal optimizations of T-shaped fin based on entransy dissipation rate minimization and maximum thermal resistance minimization. Sci China Tech Sci, 2011, 41(7): 962–970
64 Xiao Q, Chen L, Sun F. Constructal entransy dissipation rate and flow-resistance minimizations for cooling channels. Sci China Tech Sci, 2010, 53(9): 2458–2468
65 Wei S, Chen L, Sun F. Constructal entransy dissipation rate minimization of round tube heat exchanger cross-section. Int J Therm Sci, 2011, 50(7), 1285–1292
66 Xiao Q, Chen L, Sun F. Constructal design for a steam generator based on entransy dissipation extremum principle. Sci China Tech Sci, 2011, 54(6): 1462–1468